NUREG/CR-4871
SAND86-2483
R3,R4,R7
Printed June 1987

Results From the DCH-1 Experiment

W. W. Tarbell, J. E. Brockmann, M. Pilch, J. W. Ross,
M. S. Oliver, D. A. Lucero, T. E. Kerley, F. E. Arellano,
R. D. Gomez

Prepared by
Sandia National Laboratories
Albuquerque, New Mexico 87185 and Livermore, California 94550
for the United States Department of Energy
under Contract DE-AC04-76DP00789

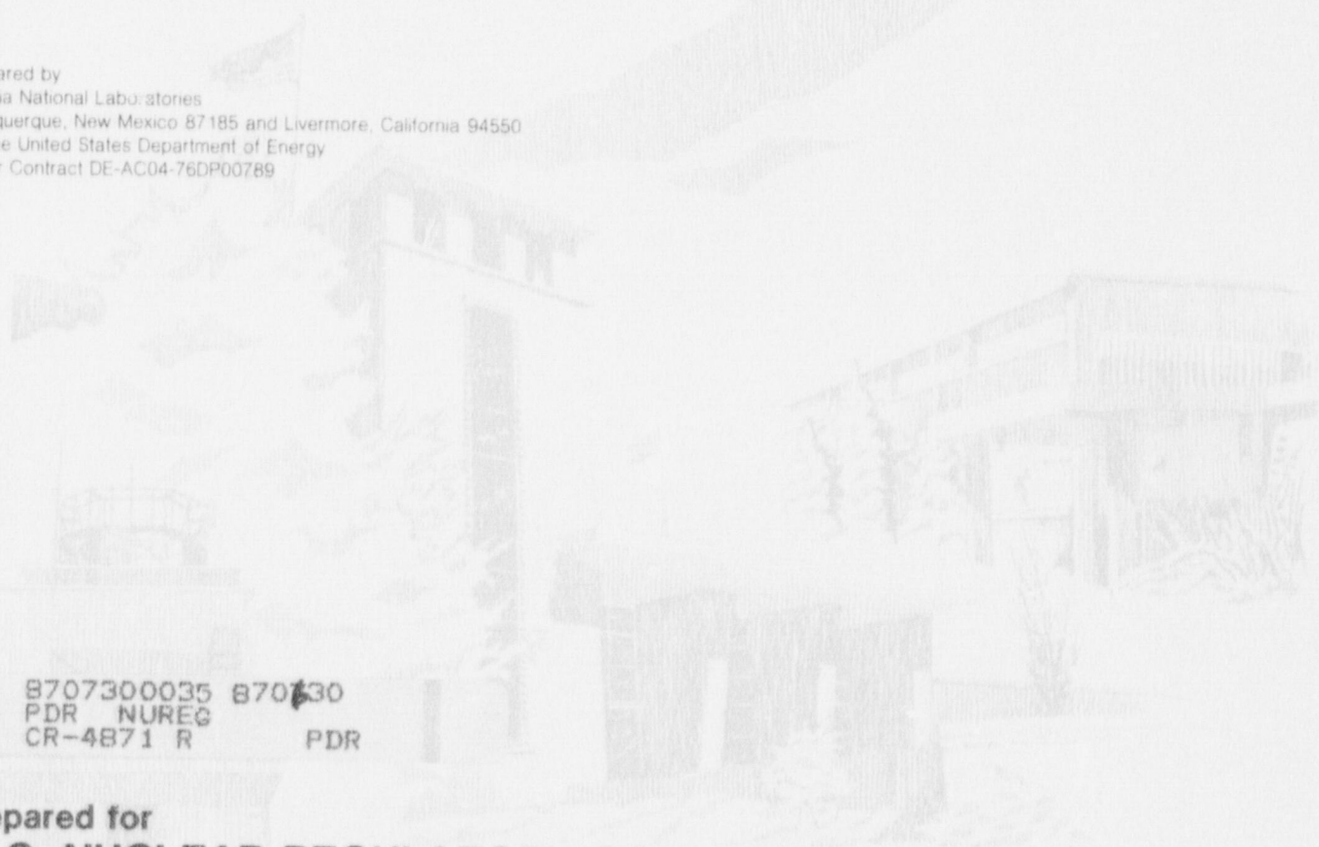

Prepared for
U. S. NUCLEAR REGULATORY COMMISSION

Available from

Superintendent of Documents
U.S. Government Printing Office
Post Office Box 37082
Washington, D.C. 20013-7082

and

National Technical Information Service
Springfield, VA 22161

NUREG/CR-4871
SAND86-2483
R3,R4,R7

RESULTS FROM THE DCH-1 EXPERIMENT

William W. Tarbell
John E. Brockmann
Marty Pilch
James E. Ross*
Michael S. Oliver*
Daniel A. Lucero
Thomas E. Kerley
Frank E. Arellano
Richard D. Gomez

May 1987

Sandia National Laboratories
Albuquerque, NM 87185
Operated By
Sandia Corporation
for the
U.S. Department of Energy

Prepared for
Division of Reactor System Safety
Office of Nuclear Regulatory Research
U.S. Nuclear Regulatory Commission
Washington, DC 20555
NRC FIN No. A1406

* Ktech Corp.

ABSTRACT

The DCH-1 (Direct Containment Heating) test was the first experiment performed in the Surtsey Direct Heating Test Facility. It produced experimental data required to understand the phenomena associated with pressurized melt ejection and direct containment heating. The results will be used to develop phenomenological models for containment response codes.

The test involved 20 kg of molten core debris simulant ejected into a 1:10 scale model of the Zion reactor cavity. The melt was produced by a metallothermic reaction of iron oxide and aluminum powders to yield molten iron and alumina. The cavity model was placed so that the emerging debris would propagate directly upwards along the vertical centerline of the chamber.

Results from the experiment showed that the molten material was ejected from the cavity as a cloud of particles and aerosol. The dispersed debris caused a rapid pressurization of the 103-m^3 chamber atmosphere. Peak pressure from the six transducers ranged from 0.09 to 0.13 MPa (13.4 to 19.4 psig) above the initial value in the chamber. The time interval from the start of debris ejection to pressure peak was on the order of two to three seconds. Posttest debris collection yielded 11.6 kg of material outside the cavity, of which approximately 1.6 kg was attributed to the uptake of oxygen by the iron particles. Mechanical sieving of the recovered debris showed a lognormal size distribution with a mass mean size of 0.55 mm. Aerosol measurements indicated a substantial portion (~2 to ~16%) of the ejected mass was in the size range less than 10 μm aerodynamic equivalent diameter.

CONTENTS

LIST OF ILLUSTRATIONS

(Continued)

LIST OF ILLUSTRATIONS (Continued)

LIST OF TABLES

I. INTRODUCTION

Experiments and analyses have shown that during a severe reactor accident molten core debris lofted into the containment may cause direct heating of the atmosphere.[1,2] If the transfer of energy is extensive, only a fraction of the total core mass would be sufficient to threaten the integrity of some containments. The potential consequences of this accident sequence make it imperative to gain information needed in the resolution of safety issues. The experiment described in this report represents a major advance in the acquisition of necessary experimental data.

The Surtsey Direct Heating Test Facility has been designed and constructed to perform experiments where molten debris is ejected into a well-defined and contained atmosphere. The name Surtsey was derived from an island formed by volcanic eruption off the coast of Iceland. The extensive volume of the facility allows the use of large scale cavity models and realistic representatives of in-containment structures. The Surtsey test chamber permits direct measurement of the pressure and temperature increase caused by the dispersal of debris from the cavity. The chamber also enables the debris and aerosol material to be sampled and recovered.

The DCH-1 test described here was the first experiment performed in the Surtsey facility. It involved 20 kg of molten material injected into a 1:10 linear scale model of the Zion reactor cavity. This report gives a description of the test apparatus, initial conditions, test observations from camera records and visual inspection, and preliminary results.

II. TEST DESCRIPTION

The Surtsey facility is depicted in Figure 1. It consists of a pressure vessel (3-m diameter by 12 m tall) oriented vertically with the lower head flange approximately two meters above the ground. Twenty ports have been placed on the cylindrical portion of the vessel along with one port on each of the two heads (only six sidewall ports are shown on Figure 1). For the DCH-1 experiment, the 1:10 linear scale model of the Zion cavity was placed in the vessel so that the floor of the cavity was at the elevation of the lower head-to-shell weld line (Elevation 2.45 m). The cavity exit was located on the vertical centerline of the vessel and oriented so that the centerline was along a line from south to north. The concrete lined cavity was modified by the addition of a 0.36 by 0.36 m by 0.9 m tall steel "chute" attached to the exit of the cavity (at the level where the tunnel would emerge into the reactor containment). The

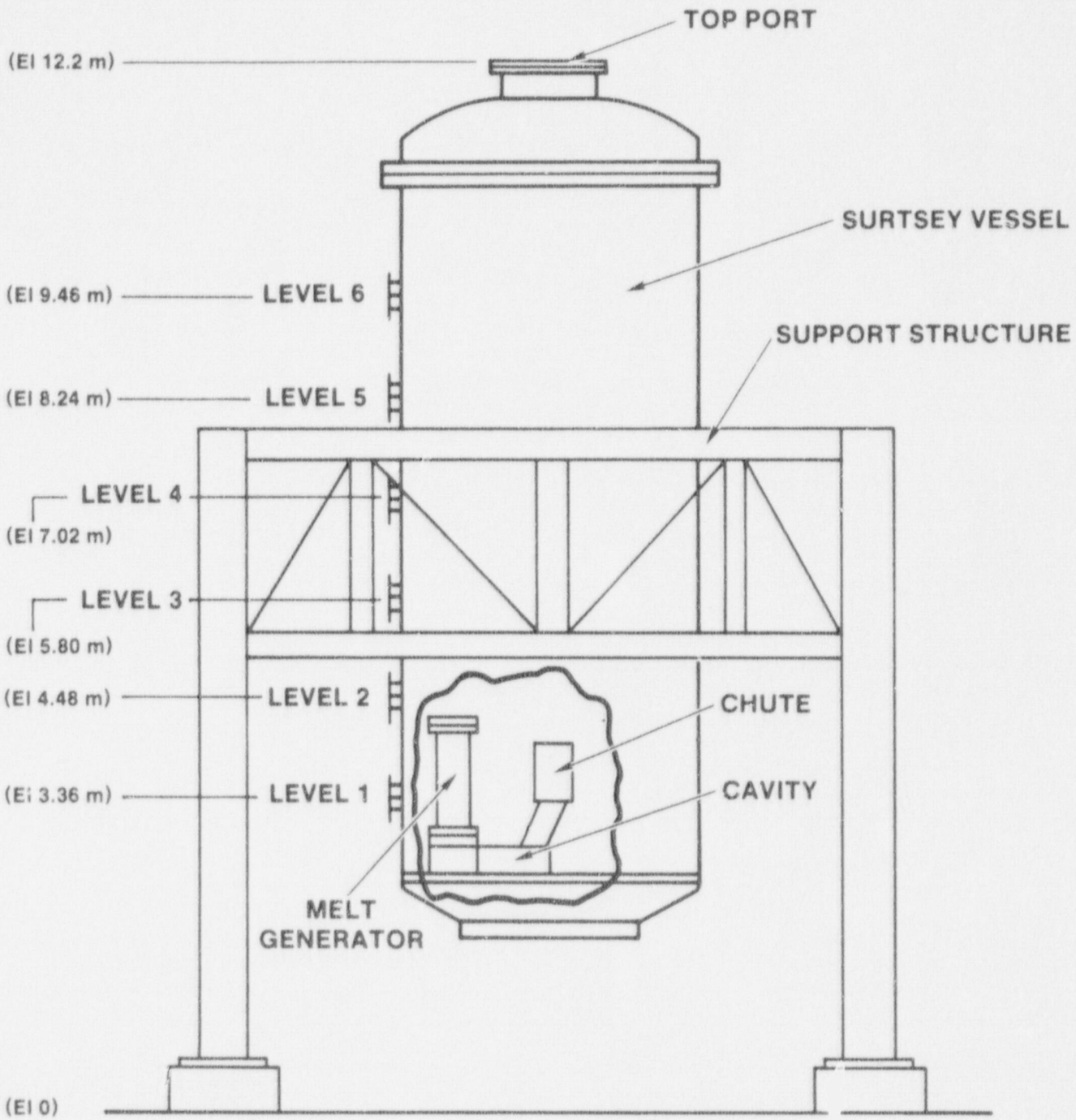

Figure 1. Schematic of the DCH-1 Apparatus In the Surtsey Direct Heating Test Facility

purpose of the chute was to direct the dispersed debris vertically upward to avoid ablation of the Surtsey steel shell. The chute terminated approximately two meters above the floor of the cavity (Elevation 4.35 m). The molten material was produced in a melt generator attached to the cavity at the scaled height of the Zion reactor pressure vessel (RPV). The annular gap around the RPV was not simulated.

The chamber and cavity were instrumented with the devices described in Table 1. The emphasis of the instrumentation was to quantify the pressure increase caused by the dispersed debris and to assess the generation of aerosol. The extensive aerosol instrumentation was designed to measure the mass concentration, size and number distributions, chemical composition, and dynamic shape factors of the aerosol particles. These data will be required to develop a source term model for this type of accident situation.

TABLE 1
DCH-1 Instrumentation

Device	Location	Range	Remark
Pressure Transducer	Melt Gen	0-1000 psig	Driving pressure
Bourdon Tube Gauge	Port N-1*	0-100 psig	Vessel pressure
Pressure Transducer	Port S-1	0-100 psig	Vessel pressure
"	"	"	
"	Port S-3	"	
"	"	"	
"	Port S-5	"	
"	"	"	
Thermocouple	Melt Gen	300-1400 K	Gas temperature
"	Port S-1	"	Vessel temperature

(Continued)

TABLE 1 (continued)

Device	Location	Range	Remark
Thermocouple	Port S-3	300-1400 K	Vessel temperature
"	Port S-5	"	" "
Pyrometer	Port S-2	1500-3800 K	Debris temperature
High-speed camera	Port S-2	200 fps	
"	Top Port	200 fps	
TV camera	Port S-2 & Top Port	30 Hz	Chamber viewing
"	Control Center	30 Hz	Overall viewing
Filter Samples	Ports E-2 & E-4 (6 ea)	-	Aerosol mass concentration
Impactors	" (4 ea)	0.1-<10 μm	Size distribution
Cascade Cyclone	Port E-4	-	Size segregated bulk aerosol
Aerodynamic Particle Sizer (APS)	Port E-5	-	Real-time particle size distribution
Photometer	Port E-4	-	Real-time mass concentration
Gas Samples	Port E-1	-	Chamber gas composition

*Port locations: N - north, S - south, E - east, W - west; elevations: 1 @3.36 m, 2 @4.58 m, 3 @5.80 m, 4 @7.02 m, 5 @8.24 m, 6 @9.46 m. For example: S-1 is a south facing flange at Elevation 3.36 m.

The six pressure transducers (Kulite Model XTE-190) and three thermocouples (Type K with 1.6-mm diameter stainless steel sheaths) that measured the chamber atmosphere were located in 12" flanged penetrations in the vessel sidewall (at Elevations 3.36, 5.80, and 8.24 m). The pressure sensors were placed in tapped holes in the steel flange cover so that the sensing element was slightly recessed in a cavity (approximately 1-cm diameter by 2.5-cm deep). The cavity was filled with stainless steel turnings to provide protection against debris particles in the atmosphere. This arrangement placed the sensing element nominally 30 cm outboard from the shell surface. The sheathed thermocouples were inserted in 6.4-mm (1/4") diameter tubing to reduce their flexibility. The exposed sensing junction was located approximately 15 cm inward from the vessel sidewall.

The pressure gauge (Kulite Model HEM-375) and thermocouple (Type K with 3.2-mm diameter stainless steel sheath) placed in the melt generator measured the condition of the gas in the free volume above the molten pool. The devices recorded the conditions prior to the start of the test, the change that occurred during the thermite reaction, and the blowdown of the gas following failure of the fusible plug. The pyrometer (Ircon Model R-35C10) was a two-color device (λ = 0.7 and 1.05 μm) focused just above the exit of the chute to detect the temperature of the ejected debris. The accuracy of the device is estimated to be on the order of ±50°C. The device was placed outside the chamber behind a clear acrylic port cover. The cover material had only a slight attenuation of light at the two operating frequencies and was subsequently calibrated against a known source. Assuming the debris radiated as a grey-body allowed the temperature to be determined without knowing the actual emittance. A high-speed motion picture camera was also positioned at this location and on the top port located on the upper head.

The aerosol devices were placed into large diameter steel pipes (flanges E-2 and E-4) so that the sampling location was near the vertical centerline of the vessel. The filter samplers (Millipore Type LS 47-mm diameter) were connected to the chamber and controlled with an isolation valve on the vacuum suction line. By controlling the valve, the sampling period of the device was determined precisely. The cascade impactors (Andersen Mk-II) and cascade cyclone (Sierra Series 280) were also controlled in the same manner. Heavy wall pipes (0.25-m diameter) attached to a port and extending into the chamber protected the wiring and tubing connected to the aerosol devices.

III. INITIAL CONDITIONS

The initial conditions for the DCH-1 test are summarized in Table 2. The melt mass was less than the 80-kg quantity used on

TABLE 2
DCH-1 Initial Conditions

Melt Mass	20.0 kg
Thermite Composition	Iron Oxide* (Fe_3O_4) 76.2 w/o plus Aluminum** (Al) 23.8 w/o
Melt Composition (fully reacted)	Iron (Fe) 55.2 w/o plus Alumina (Al_2O_3) 44.8 w/o
Dopants	Lanthanum Oxide (La_2O_3) - 118 g Barium Molybdate ($BaMoO_4$) - 313 g Niobium pent-oxide (Nb_2O_5) - 143 g Nickel (Ni) - 100 g
Ambient Temperature	26°C
Ambient Pressure	0.08 MPa (12.0 psia)
Driving Gas	Dry bottled nitrogen (N_2)
Melt Generator Gas Volume	0.109 m^3 (41.1-cm diameter by 156.7 cm long)
Initial Gas Pressure	1.86 MPa (270 psig)
Fusible Plug Diameter	4.8 cm

* Chemalloy MS-30 (100% minus 30 mesh)
** ALCOA Atomized Powder (flake form)

previous HIPS (High Pressure Melt Streaming) tests[1] to reduce the extent of direct atmosphere heating to a level calculated to be within the capacity of the Surtsey vessel. The thermite weight fractions stated in the table are for the base melt composition, without correction for the dopant mass. The gas volume of the melt generator was larger than in previous tests because of the reduced mass occupied by the thermite.

The dopants placed in the melt were designed to simulate the chemical behavior of several classes of radionuclides. The total mass of these simulants was limited to prevent significant depression of the melt temperature. The mass of the brass fusible plug (292 g) also contributed about 1.5 w/o of copper and 0.8 w/o of zinc to the initial mass of the melt.

IV. TEST OBSERVATIONS

The principal test observations were obtained by three TV cameras: one viewing the overall apparatus, a second located on the top port looking into the vessel, and a third focused on the large-face Bourdon tube gauge. The first two devices were designed primarily for observation to ensure safe operation during the experiment. The latter device gave an immediate indication of the pressure within the chamber although the response of the gauge was slower than the transducers placed in the chamber.

Upon ejection of the melt into the atmosphere of the vessel, the top mounted camera recorded a brilliant flash that lasted several seconds. This was followed by virtually total darkness within the chamber. The Bourdon tube gauge was observed to rapidly sweep to a value of approximately 15 psig (0.1 MPa) before decaying to around 2-3 psig (~0.01-0.02 MPa) in a few seconds. No observable changes were detected with the overall video camera that viewed the outside of the chamber.

When the chamber pressure stabilized at nominally 1 psig (approximately 15 min after the test), experimenters examined the facility to assess possible damage to the equipment. No obvious damage was detected. It was observed through the camera ports that the chamber was filled with suspended aerosol particles that appeared to move in random directions. Most of the upward facing horizontal surfaces in the chamber were covered with a thick layer (~1 mm) of light-brown particulate. Aerosol was also detected in the dilution box used in conjunction with the aerodynamic particle sizer (APS) system (TSI Model 33).

When the chamber was opened the day following the test, the presence of the thick aerosol layer was confirmed. All exposed horizontal surfaces were heavily covered with the fine, loose particulate material. The vertical shell wall and the underside of the top head also displayed a somewhat thinner coating of fine particles. A few large globules of frozen melt (several cm mean dimension) were found atop the cavity apparatus but nowhere else in the chamber. A thin layer of melt was attached to the underside of the aerosol pipe enclosure at Level 4 and on one side of the top head. Debris particles were observed on horizontal surfaces and the floor among the settled aerosol.

V. TEST RESULTS

A. Melt Generator

The melt generator pressure record is given in Figure 2. The record was from 20 s prior to melt ejection (zero time) to 10 s afterwards. The determination of the actual zero time was difficult because the optical probe placed on the fusible plug did not function. Zero time was established for the plots as the point in time where pressure first began to decrease. It is estimated that actual time of ejection differed by the time used by no more than 20 ms.

Based on the melt generator pressure, the total thermite reaction time was somewhat less than 8 s. This was comparable to previous HIPS experiments[2] considering the reduced height of the thermite powder bed. The total height in this test was decreased by a factor of four. The "dip" in pressure just after ignition was not expected and had not been observed in any previous test. Inspection of the melt generator thermocouple record (Figure 3) showed a similar, but inverted, pulse occurring at the same time. This behavior suggested electrical interference as the cause of the dip. The other gauge records also indicated the same effect, although much less pronounced.

The influence of the electrical interference on the remainder of the melt generator pressure record was not known. The thermocouple and other pressure gauges appeared to return to the pretransient state following the duration of the interference (on the order of 1.6 seconds). For this reason, the recorded peak pressure and blowdown history were believed to be accurate. Thus, the pressure at the time of ejection was 2.55 MPa (370 psig), representing a 37% increase in pressure during the thermite reaction.

B. Melt Temperature

The recorded debris temperature obtained with the two-color pyrometer is given in Figure 4. The plot shows an initial increase in temperature prior to the zero time established by the pressure record. This indicated that at least part of the debris dispersal occurred prior to a detectable drop in the melt generator pressure. The duration of the debris ejection was indicated to be on the order of 1.1 s. Peak temperatures approaching 2000°C were recorded at 0.1 s. These values were slightly less than observed in several previous HIPS tests.[1] The two records on the plot indicate the data as recorded and corrected for the influence of the 2.5 cm thick acrylic port window. The correction factor was determined by a posttest calibration of the pyrometer with and without the window in

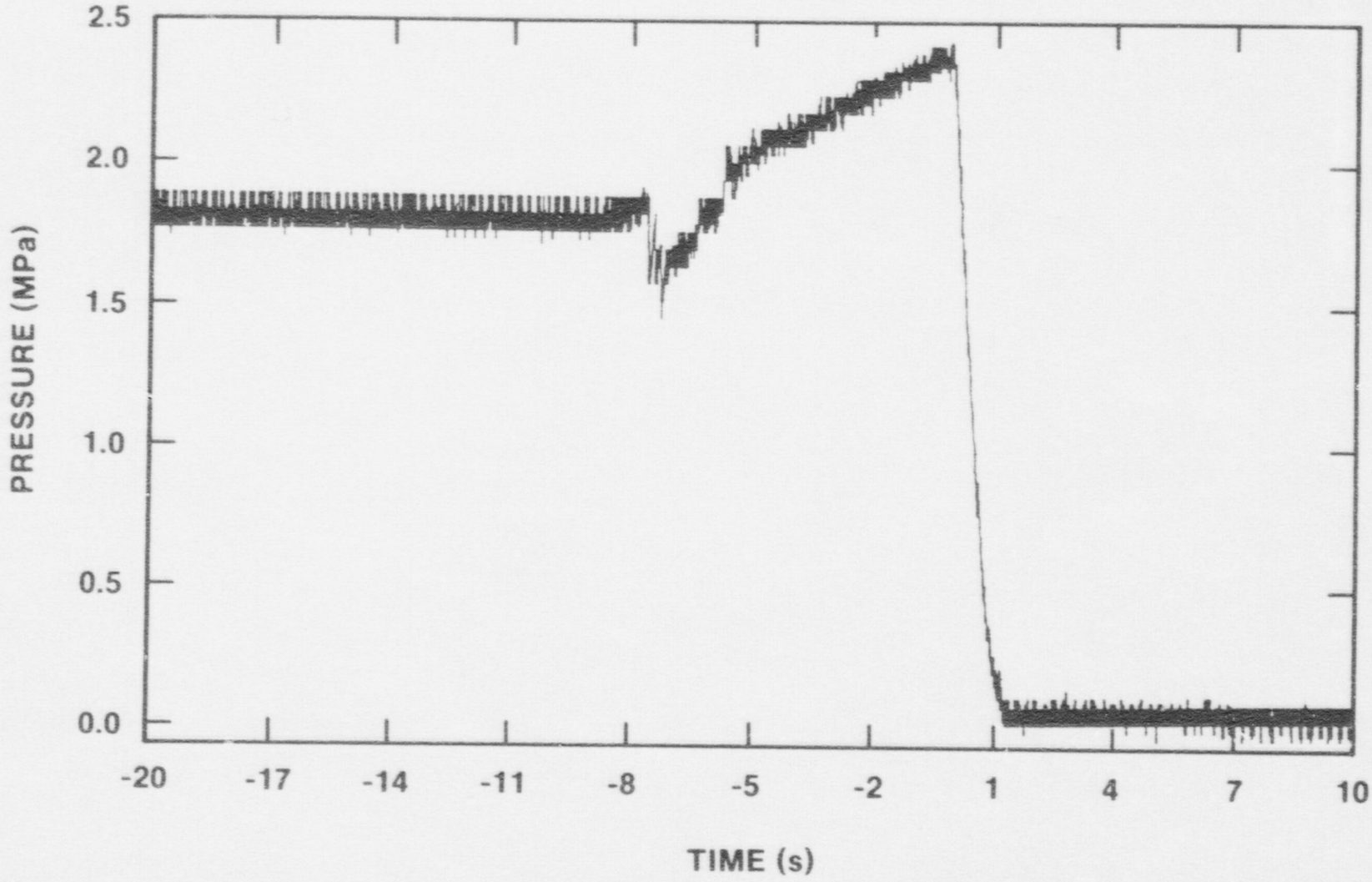

Figure 2. Melt Generator Pressurization History

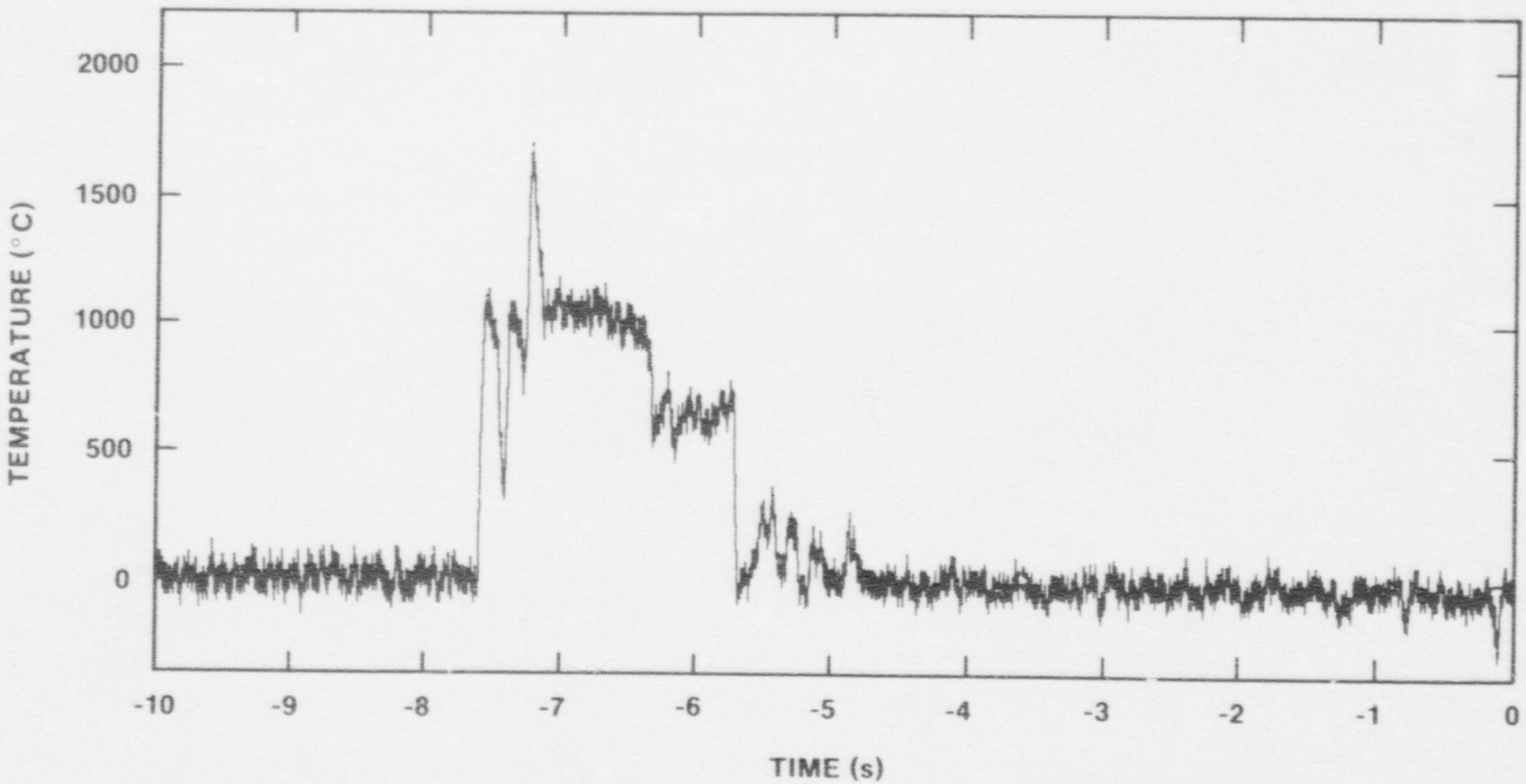

Figure 3. Melt Generator Thermocouple Record

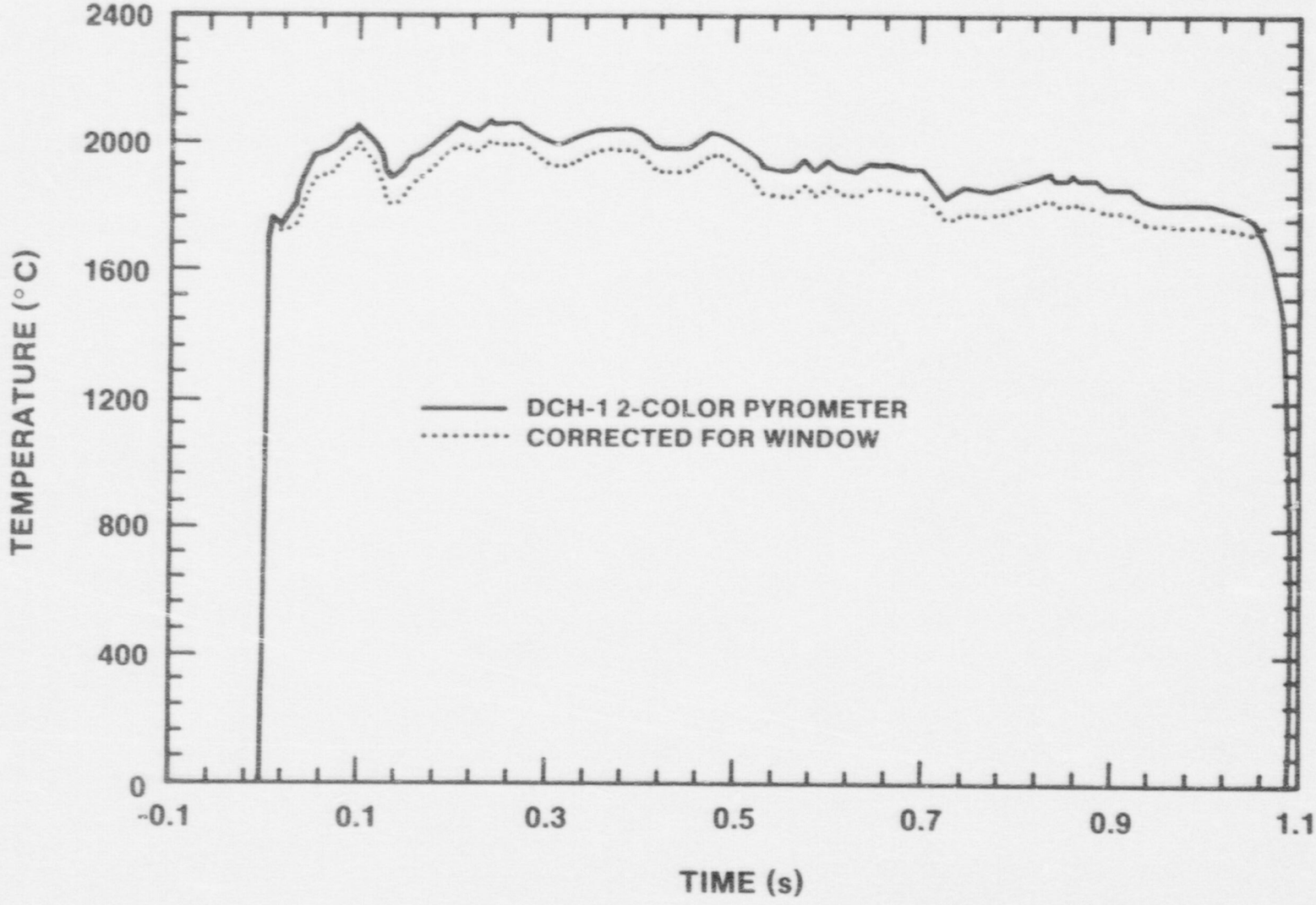

Figure 4. Dispersed Debris Temperature

place. The slightly nonlinear correction function caused the recorded temperatures to be reduced approximately 50°C. Some additional heat loss may have occurred because of the longer path length with the addition of the chute. The reduced melt mass of the reacted thermite caused an increase in the surface area to volume ratio that may have enhanced the losses within the melt generator.

C. Chamber Response

Two pressure gauges and one thermocouple were placed in each of three ports on the shell portion of the Surtsey vessel. The ports were along a vertical line oriented in the southwest direction and were referred to as bottom, middle, and top to identify Levels 1,3, and 5, respectively. The recorded pressure histories for the six gauges are given in Figures 5-10. The pressure values were obtained using the manufacturer's stated sensitivity. The calibration of each gauge was checked after the test and all were within 1% of their pretest value. The recorded data show electrical noise superimposed on the measured signal. Because of this, the zero pressure baseline was not clear on some of the records. Estimates of the peak pressure from each plot are given in Table 3.

Most of the gauge records demonstrated pronounced electrical interference, before and after the pressure transient. The cause of the interference was ground loop currents circulating through the vessel and instrument cables. The decay portion of the curves showed a cyclic pattern characteristic of several different frequencies forming harmonic behavior. The range of the frequencies was too high to be attributed to a mechanical phenomena such as vibration of the vessel.

All of the plots were characterized by a rapid increase in pressure (80-90% of the peak value in about one second) with the peak value occurring at nominally three seconds. The slope of the pressure profile on either side of the peak was nearly symmetric to about 80% of the maximum value. Following this, the decay in pressure (without the interference pattern) was virtually exponential in form. Based on this assumption, an estimated time constant was found for each record. The values presented in Table 3 show that the apparent decay time constant was on the order of 30-40 s. This range was at least ten times shorter than the leak rate determined prior to the test.

The pressure data from gauge P-3 were somewhat higher than the other records. The posttest gauge calibration indicated that the sensitivity of the gauge changed approximately one percent from the manufacturer's quoted value. The cause of the higher pressure readings from this gauge is not certain but its location

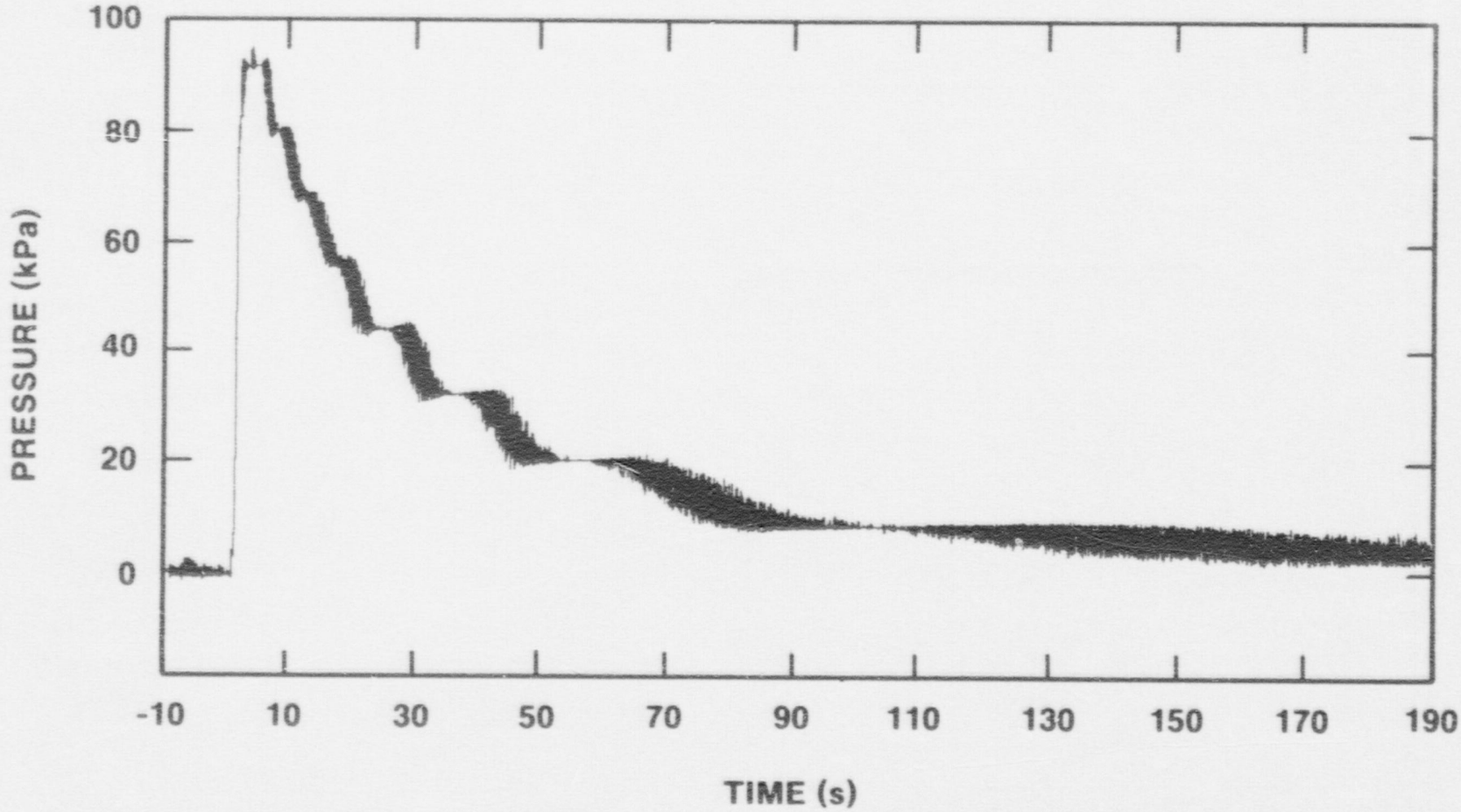

Figure 5. Surtsey Chamber Pressure - Gauge P-2

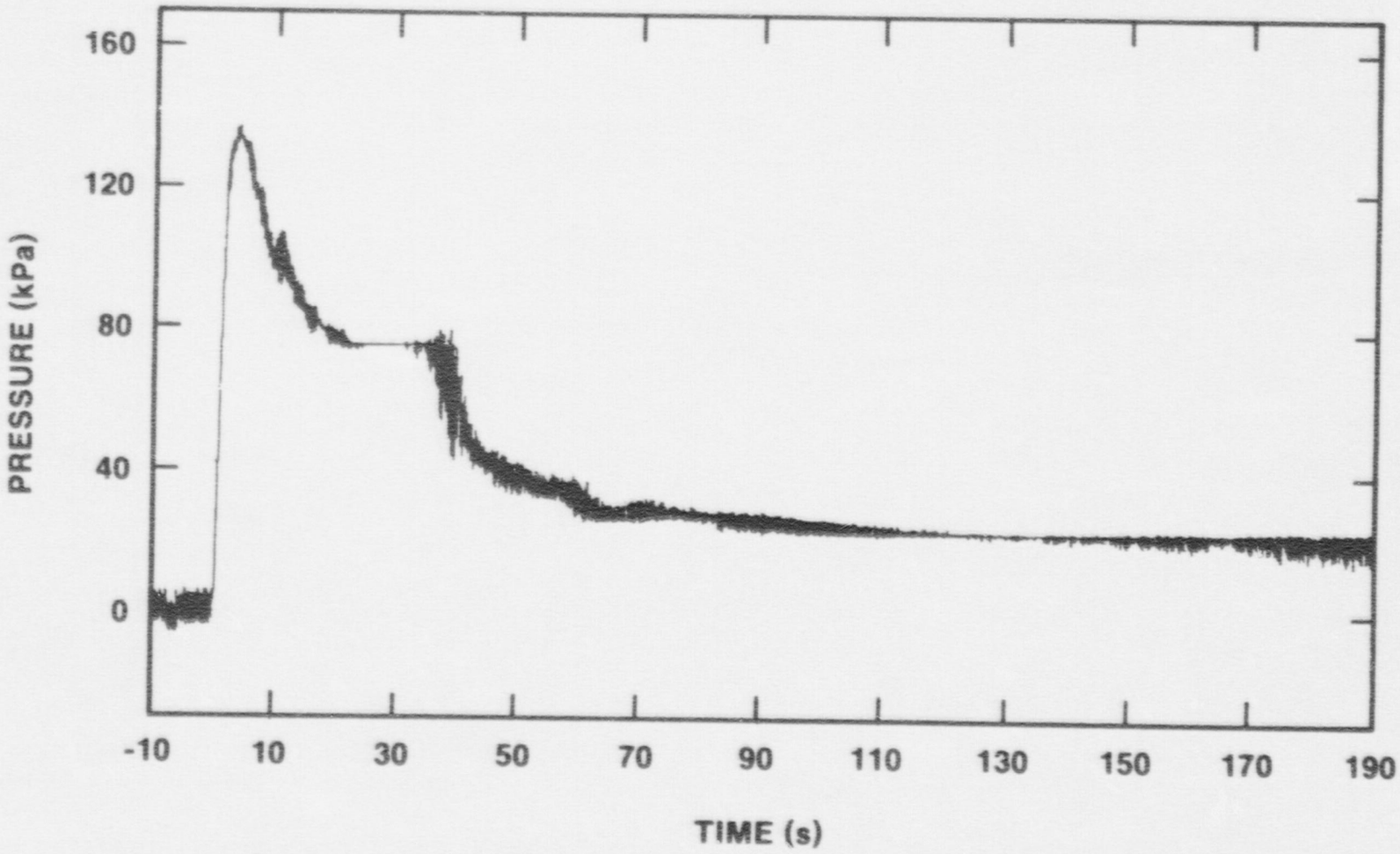

Figure 6. Surtsey Chamber Pressure - Gauge P-3

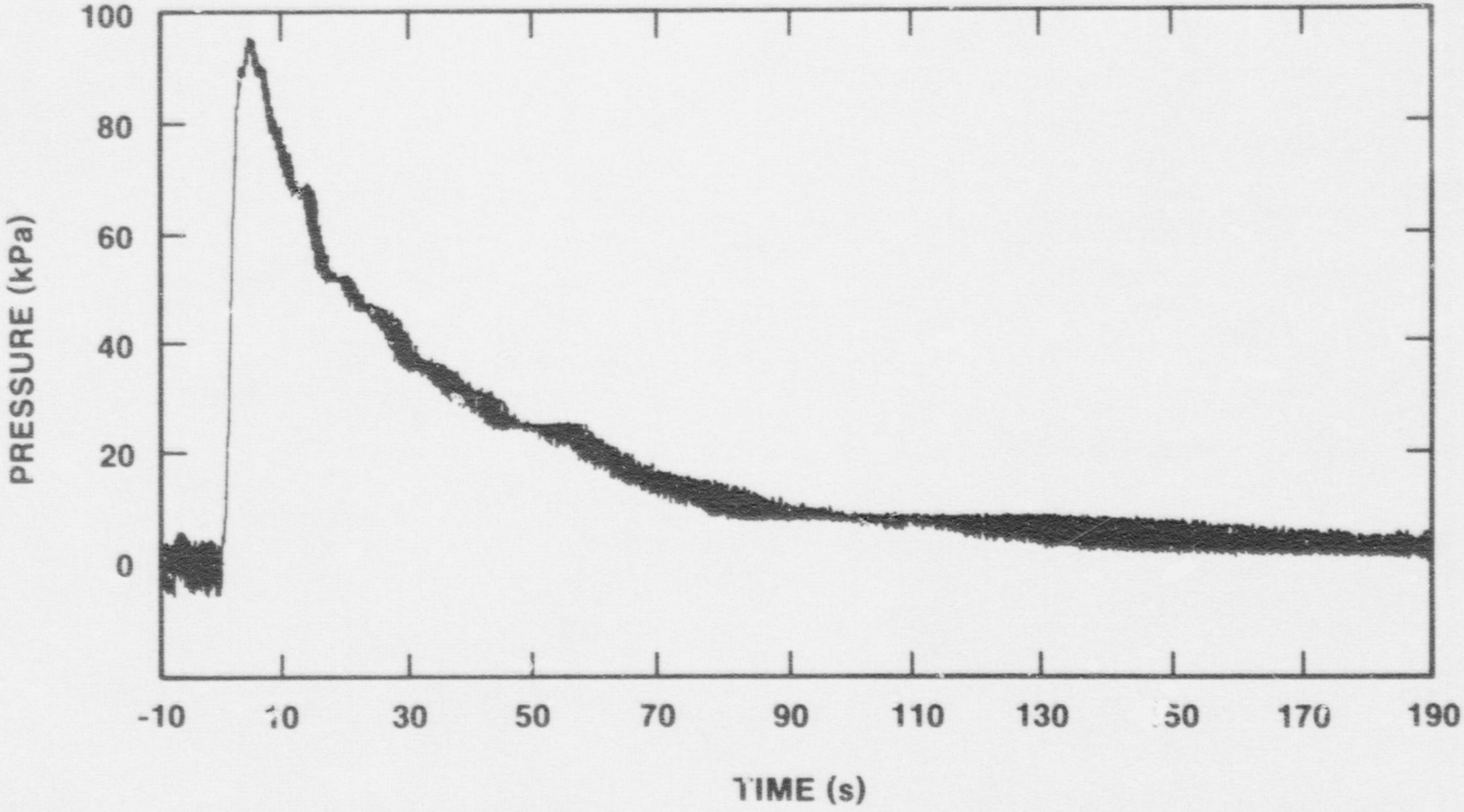

Figure 7. Surtsey Chamber Pressure - Gauge P-4

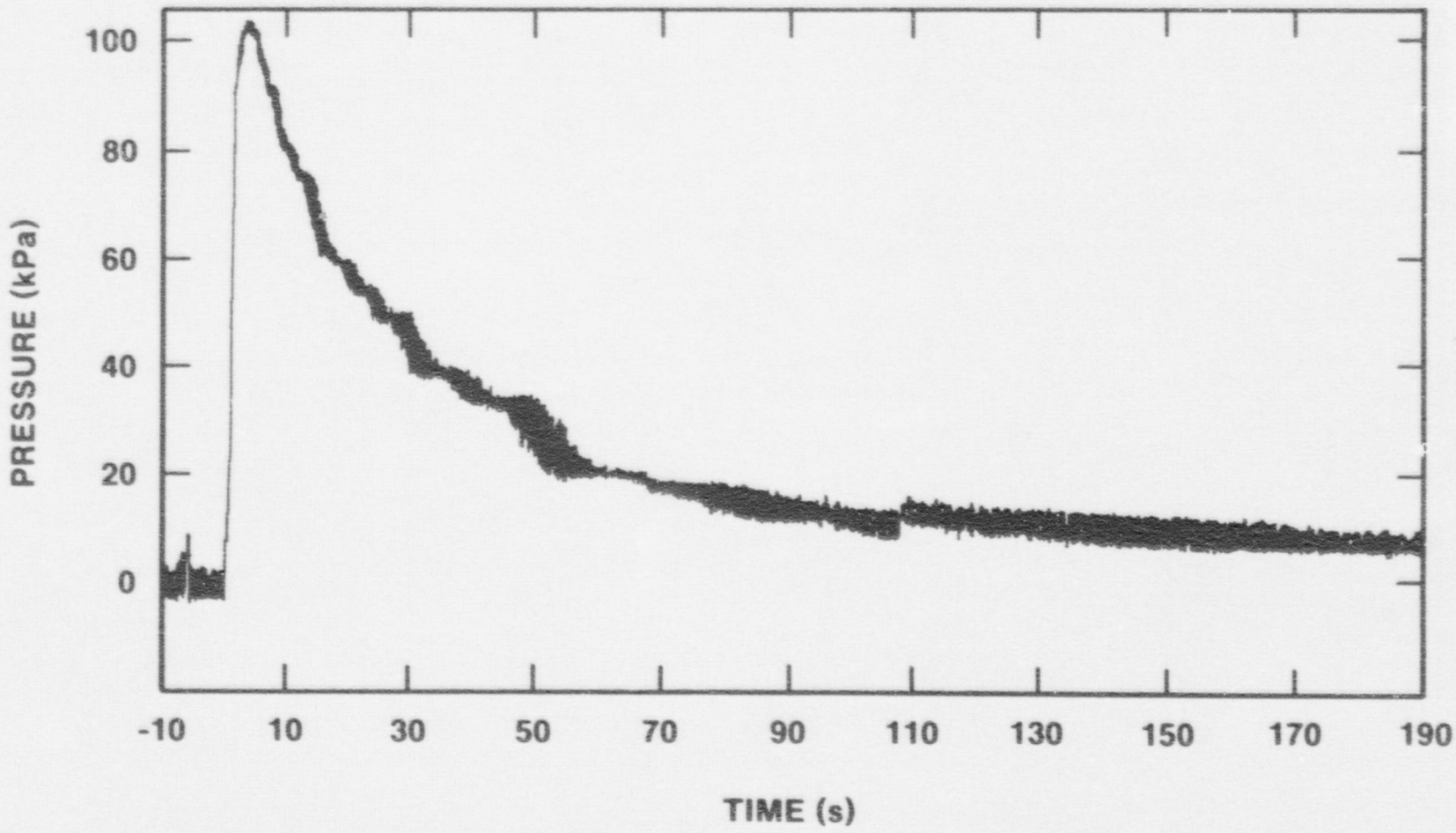

Figure 8. Surtsey Chamber Pressure - Gauge P-5

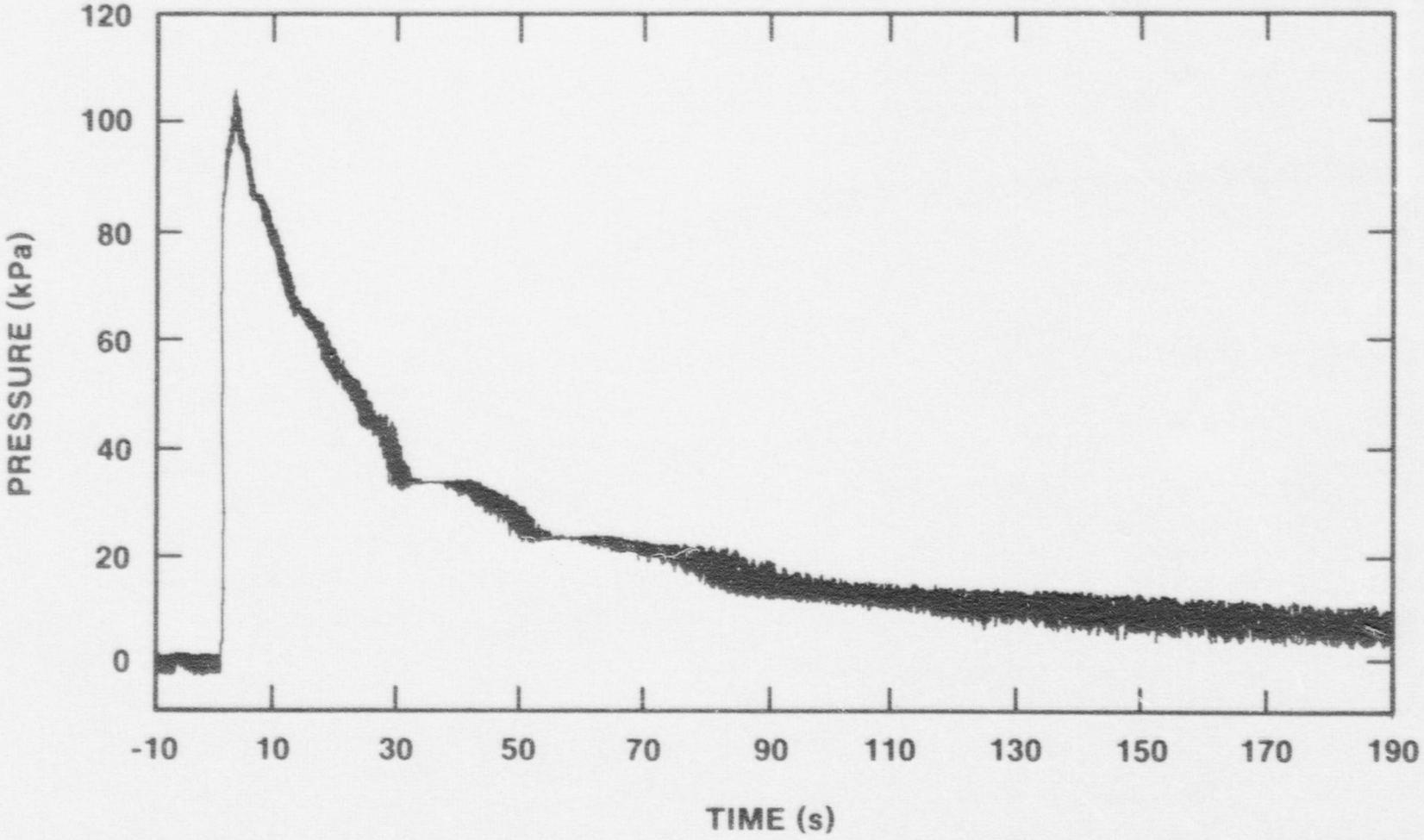

Figure 9. Surtsey Chamber Pressure - Gauge P-6

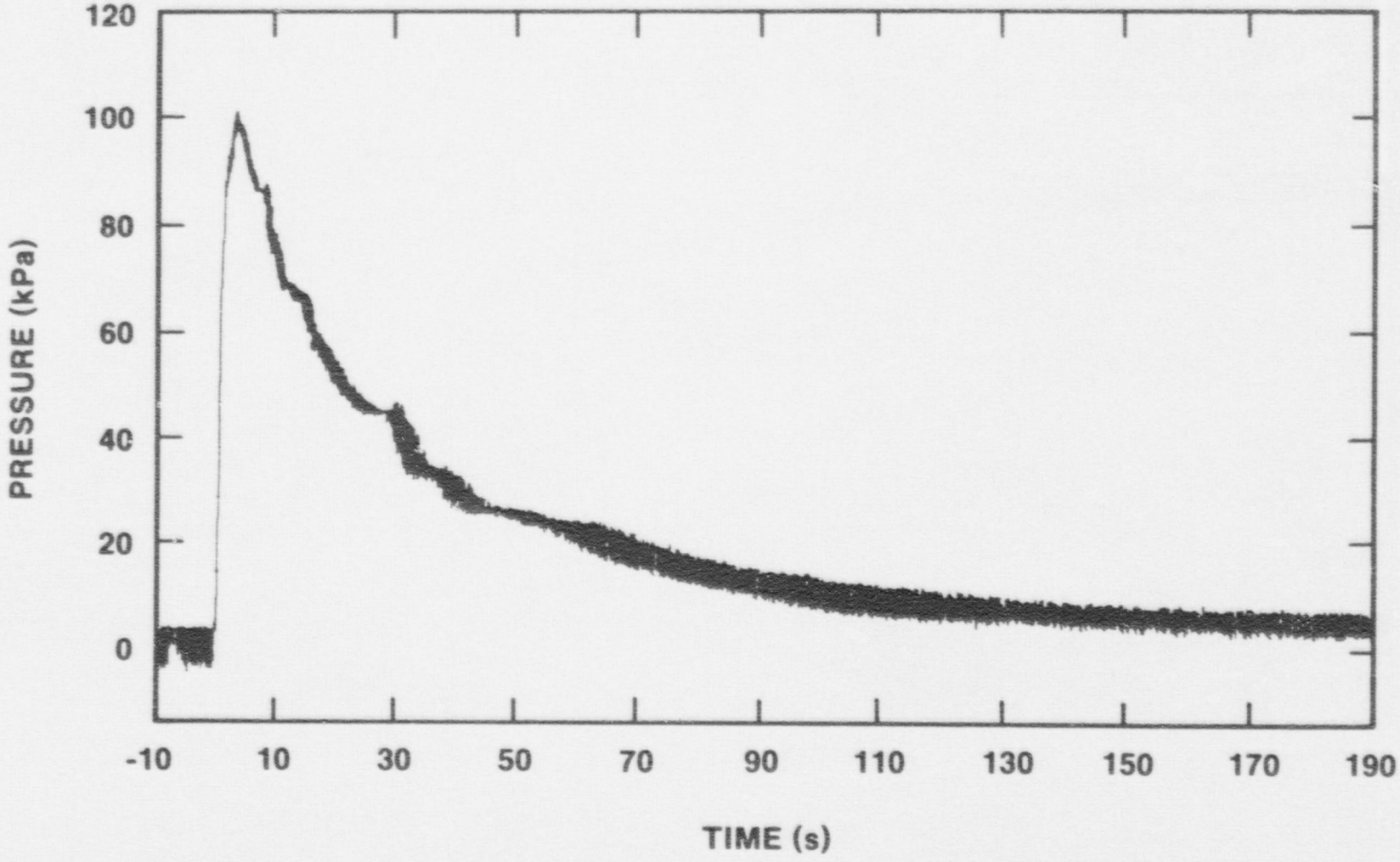

Figure 10. Surtsey Chamber Pressure - Gauge P-7

placed it close to the debris source. Exposure of the sensing element to elevated temperature material could cause ambiguous response. Typically heat flux to the gauge face will cause a greater indicated pressure than the actual value.

TABLE 3
Peak Gauge Pressure

Gauge	Port Location	Peak Pressure (MPa/psig)	Change In Temperature (°C)	Time Constant* (s)
P-2	Bottom (S-1)	0.092/13.4		31
P-3	Bottom (S-1)	0.133/19.4		42
P-4	Middle (S-3)	0.095/13.8		38
P-5	Middle (S-3)	0.100/14.6		38
P-6	Top (S-5)	0.103/15.0		28
P-7	Top (S-5)	0.098/14.2		32
T-1	Bottom (S-1)		60	100
T-2	Middle (S-3)		75	185
T-3	Top (S-5)		255	80

* $X_t = X_{peak}(e^{-t/\tau})$ where: X is pressure or temperature, t = time and τ = time constant: at $t = \tau$: $X_t = X_{peak}(e^{-1})$

The chamber atmosphere temperature histories recorded by the three thermocouples are given in Figures 11-13. The vertical axis gives the temperature increase above ambient while the time axis was extended to 190 s to demonstrate the slow decay of the temperature. The Bottom and Middle sensors recorded temperature changes that were very low, while the Top device was significantly higher. Likewise, the time constant for decay (to 1/e of the peak value) also varied considerably. The discrepancy was probably caused by deposition of debris and aerosol in the

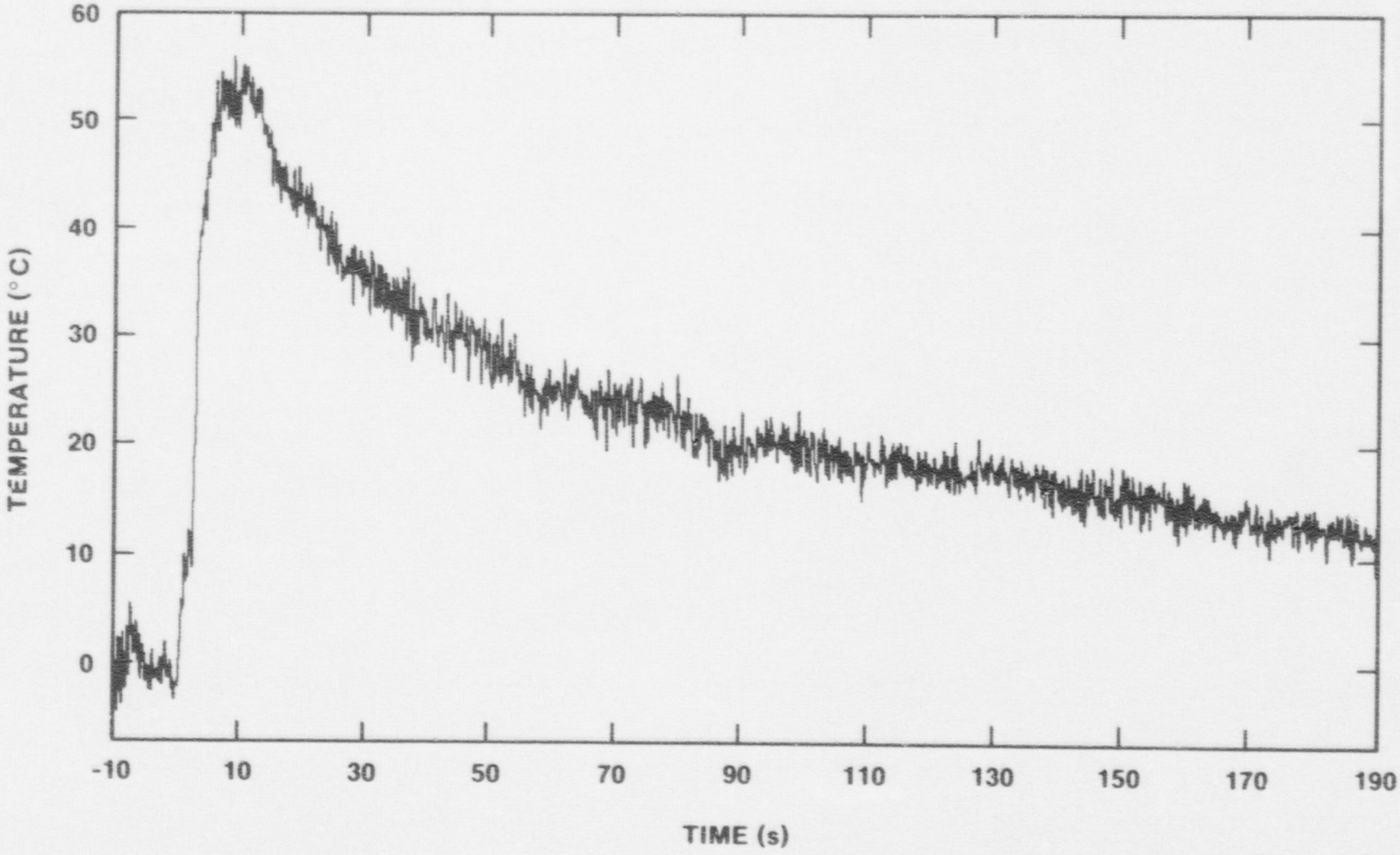

Figure 11. Surtsey Chamber Temperature - Thermocouple T-1

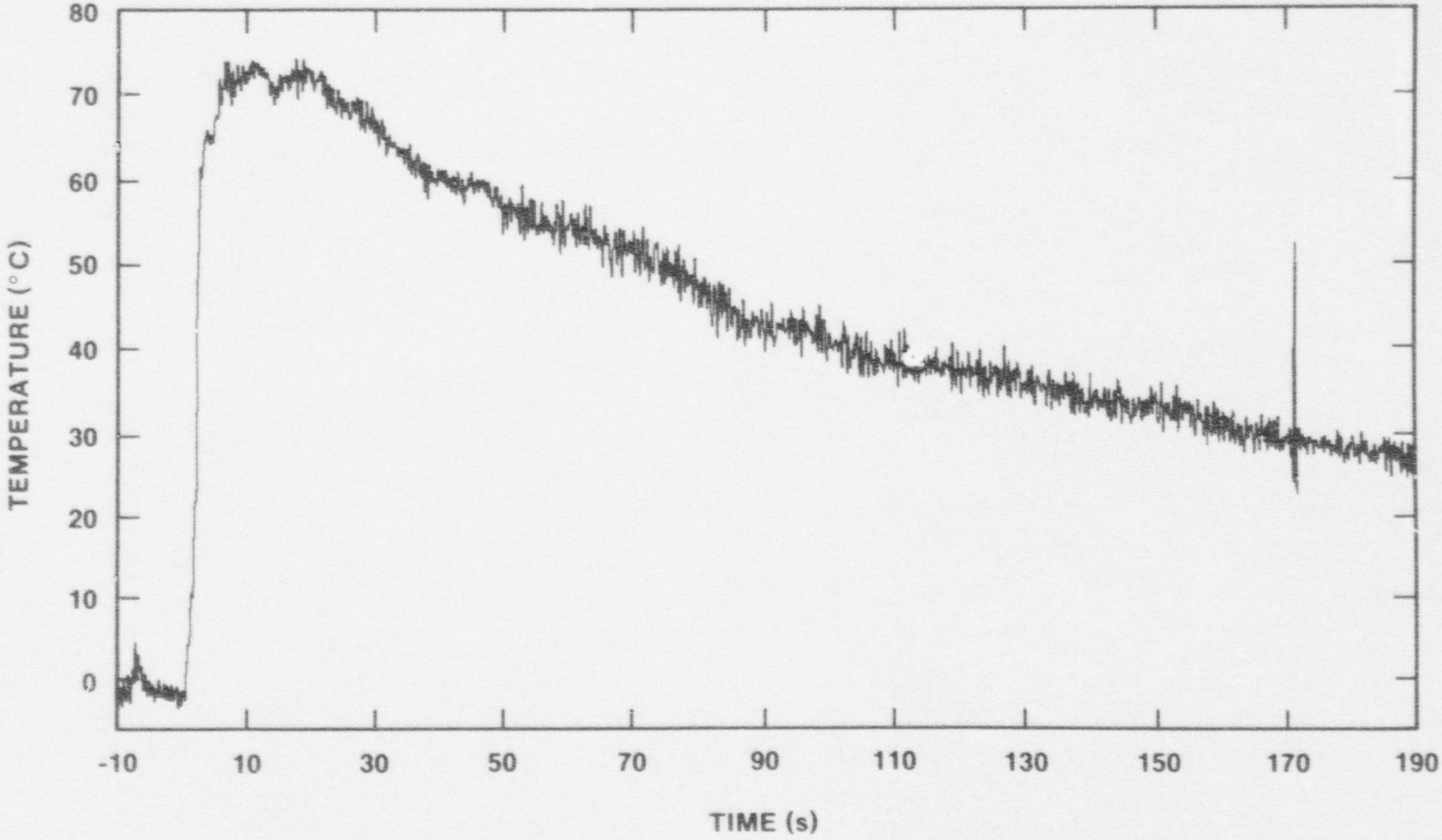

Figure 12. Surtsey Chamber Temperature - Thermocouple T-2

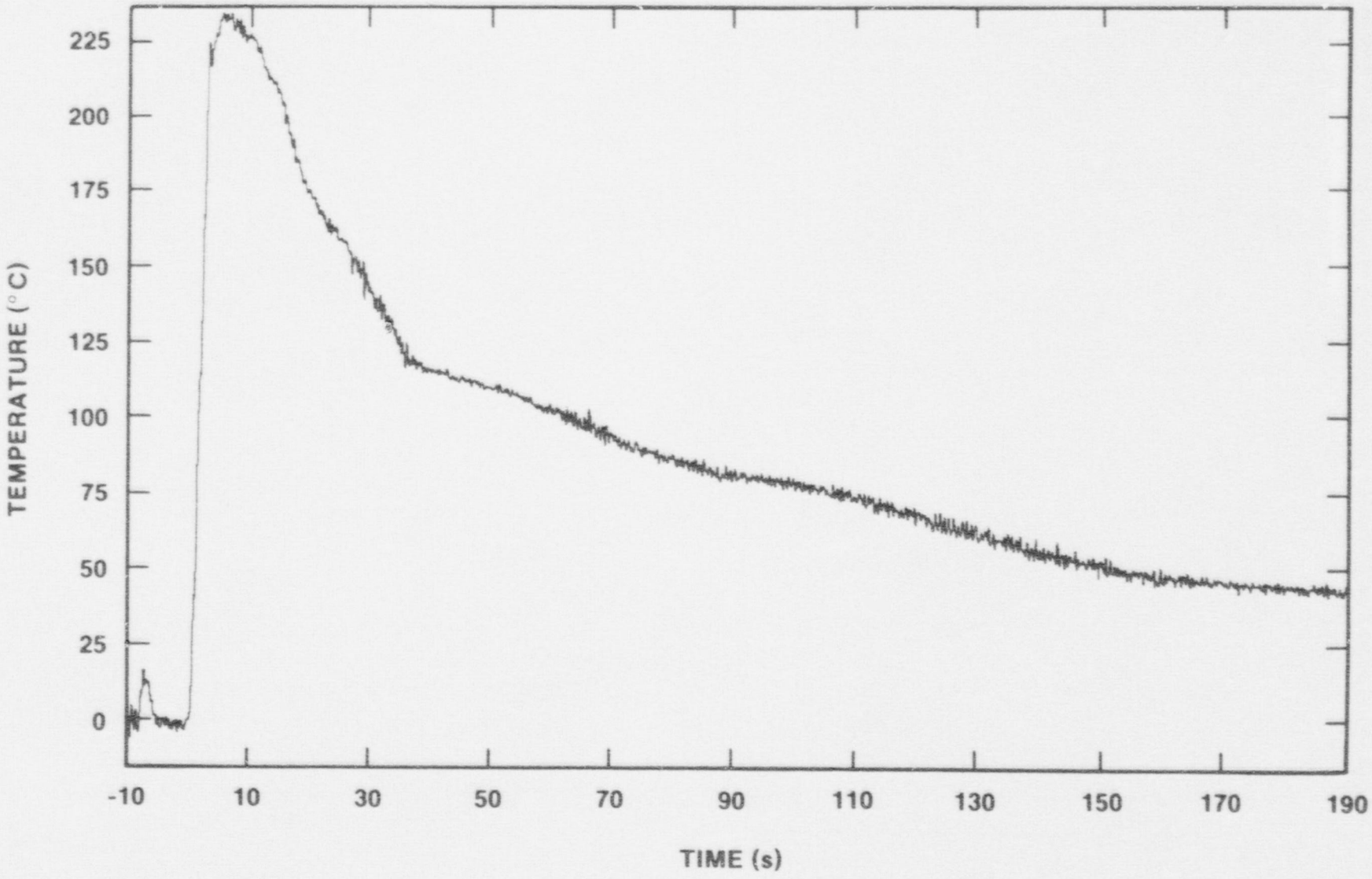

Figure 13. Surtsey Chamber Temperature - Thermocouple T-3

vicinty of the exposed sensor. Hot debris would cause a greater peak temperature to be recorded than the actual atmospheric value. Aerosol deposited later could limit the heat transfer to the sensor and reduce the effect on the gauge response.

D. Debris Characterization

The Surtsey chamber allowed collecting the debris that was dispersed from the cavity. The total mass available for dispersal is summarized in Table 4.

TABLE 4
Initial Melt Mass and Composition

Constituent	Mass (kg)	
Bulk Melt Fe and Al_2O_3		
Fe	11.000	
Al_2O_3	9.000	
Total		20.000
Fission Product Mocks		
Mo	0.101	
Ni	0.100	
La_2O_3	0.118	
BaO_4	0.161	
Nb_2O_3	0.143	
Total		0.623
Brass Fusible Plug		
Cu	0.179	
Zn	0.103	
Pb	0.009	
Total		0.292
Steel Eroded From Lower Flange		
Fe	0.200	
Total		0.200
Total Initial Melt Mass		21.115

The list in Table 4 includes the expected form of the fission product mocks after undergoing the thermite reaction. The 200-g mass of steel eroded from the generator flange was obtained by measuring the final aperture shape and calculating the removed volume.

All relocated material was collected by vacuuming the inside of the chamber. A fine particulate filter element on the unit allowed all but the smallest material (<20 μm diameter) to be retained. Material was also collected from the surfaces within the chamber that exhibited a crust layer, i.e., the underside of the aerosol pipe devices and the upper head. The crust on the underside of the top head was difficult to remove because it was thin (~1 mm) and tightly bonded to the metallic surface.

The total mass collected from the chamber yielded the amount of material dispersed from the cavity. Material retained within the cavity and melt generator was also evaluated to yield an overall mass balance. These results are summarized in Table 5.

TABLE 5
Recovered Debris Mass Balance

Location	Mass (kg)
Chamber walls and floor	10.168
Underside of top head	1.462
(a) Total Dispersed	11.630
Cavity and chute	7.963
Floor of cavity at inclined tunnel	1.177
Melt generator lower flange	0.507
(b) Total in Apparatus	9.647
Total Mass (a + b)	21.277

The material taken from the cavity and chute was in the form of a crust layer, except for the single large mass found on the floor of the cavity at the base of the inclined shaft. The crust thickness averaged 2-3 mm where it was attached to the concrete sidewalls or floor. It had the appearance of a very dense material with little porosity. Some concrete adhered to the crust layer and could not be easily removed. The crust in the steel chute was thinner (1-2 mm) and was also very dense, but with some large embedded globules. The pattern of the crust in the chute corresponded with the cavity's angle of inclination with very little detectable lateral spreading of the debris stream. Close inspection indicated that the crust in both the cavity and chute was made of fine particles tightly bonded together.

Some areas within the cavity (primarily on the floor) showed a second crust layer atop the first. This second layer was much more porous than the underlying material and had a smooth upper surface. The large mass at the base of the shaft was also of this form. This material has been identified as melt that was not entrained by the gas blowdown. Because the melt could not undergo several interactions and still escape under its own momentum, the large mass at the base of the inclined tunnel was probably from a film of material that was not carried out of the cavity. The large pores were developed as the heat from the debris decomposed the underlying concrete (chemically bound water was released but concrete melting did not occur), causing gas to escape up through the solidifying mass.

The total mass of debris collected (21.277 kg) compares favorably with the entire melt mass available (21.115 kg); however, there were several uncertainties in the mass balance analysis.

(1) Debris recovered from the cavity included an unknown amount of adhered concrete.

(2) The debris recovery process may have been incomplete.

(3) The mass removed from the chamber may have included residual material from the vessel construction that was dislodged during the test.

(4) The debris recovered from the chamber included an unknown mass of oxygen that chemically combined with the metallic constituent of the melt.

Bounding calculations on the mass of melt initially in the chamber were done based on the limits of oxygen uptake. Assuming that the mass fraction of iron was constant at 53%, then the

11.630 kg of debris recovered represented 6.16 kg of iron if no oxidation occurred. If all of the iron were oxidized to Fe_2O_3, then 5.02 kg of iron were discharged into the chamber. These figures represent a range of 46% to 56% dispersion of the initial melt mass into the chamber. These results are summarized in Table 6.

TABLE 6
Estimated Oxidation Range of Debris
Discharged Into The Chamber

Debris Oxidation State and Mass (kg)	Oxygen Uptake (kg)	Al_2O_3 Mass (kg)	Total Mass (kg)
Fe - 6.16	0.0	5.47	11.63
Fe_2O_3 - 5.02	2.16	4.45	11.63

The oxygen concentration measurements attempted in the experiment did not have sufficient accuracy to resolve the uncertainty in the extent of oxygen that reacted with the iron in the debris. Chemical analysis of the debris has shown all oxide forms within the samples tested. The complexity of this procedure prevents analyzing the entire mass of collected debris to obtain a quantification of the individual oxide states.

After the debris was collected and weighed, the material was mechanically sieved to determine particle size distribution. A Rotap 60 Automatic Sifter was employed with seven separate mesh sizes. The material collected on each sieve was then weighed to determine the mass fraction of the total material represented by that size range. The results of the sieving are given in Table 7. The material removed from the underside of the top head was not in particulate form and therefore was not included in the sieve analysis. The aerosol in the sampling devices was not included in the sieving because it was a very small mass compared to the material collected from the chamber and it was mainly in a size range less than 0.05 mm.

The results given in Table 7 have been plotted in Figure 14 along with the data from the previous SPIT-18 and SPIT-19 (System Pressure Injection) experiments.[2] The figure shows that the DCH-1 debris size distribution is lognormal and intermediate between

the two previous data sets. The calculated mass mean size is 0.55 mm with a geometric standard deviation of 4.2 .

TABLE 7
Debris Sieve Analysis

Sieve Size (mm)	Debris Mass (kg)	(%)
> 2.38	1.504	15.2
1.60-2.38	0.823	8.3
0.85-1.60	1.559	15.7
0.417-0.85	1.989	20.1
0.105-0.417	2.973	30.0
0.075-0.105	0.397	4.0
0.053-0.075	0.215	2.2
< 0.053	0.446	4.5
Total	9.906	100.0

The material recovered from the chamber was studied at high magnification to determine the geometric character of the debris. Photographs of four different size groupings are given in Figure 15 along with a brief qualitative description in Table 8. Some agglomerates were in the sieved samples collected from the chamber so that the estimated mass mean size (DGM = 0.55 mm) may be slightly larger than the airborne material.

The shrink holes seen in the particles were formed during the time the liquid drops cooled in the atmosphere. Heat transfer from the drop in the atmosphere caused a solid outer surface to form. Subsequently, the center of the drop lost heat and a large contraction occurred. The ensuing compressive stress in the outer shell was relieved by the initiation of a fissure. The irregular shapes were attributed to mechanical fracturing by cracking of large solid particles.

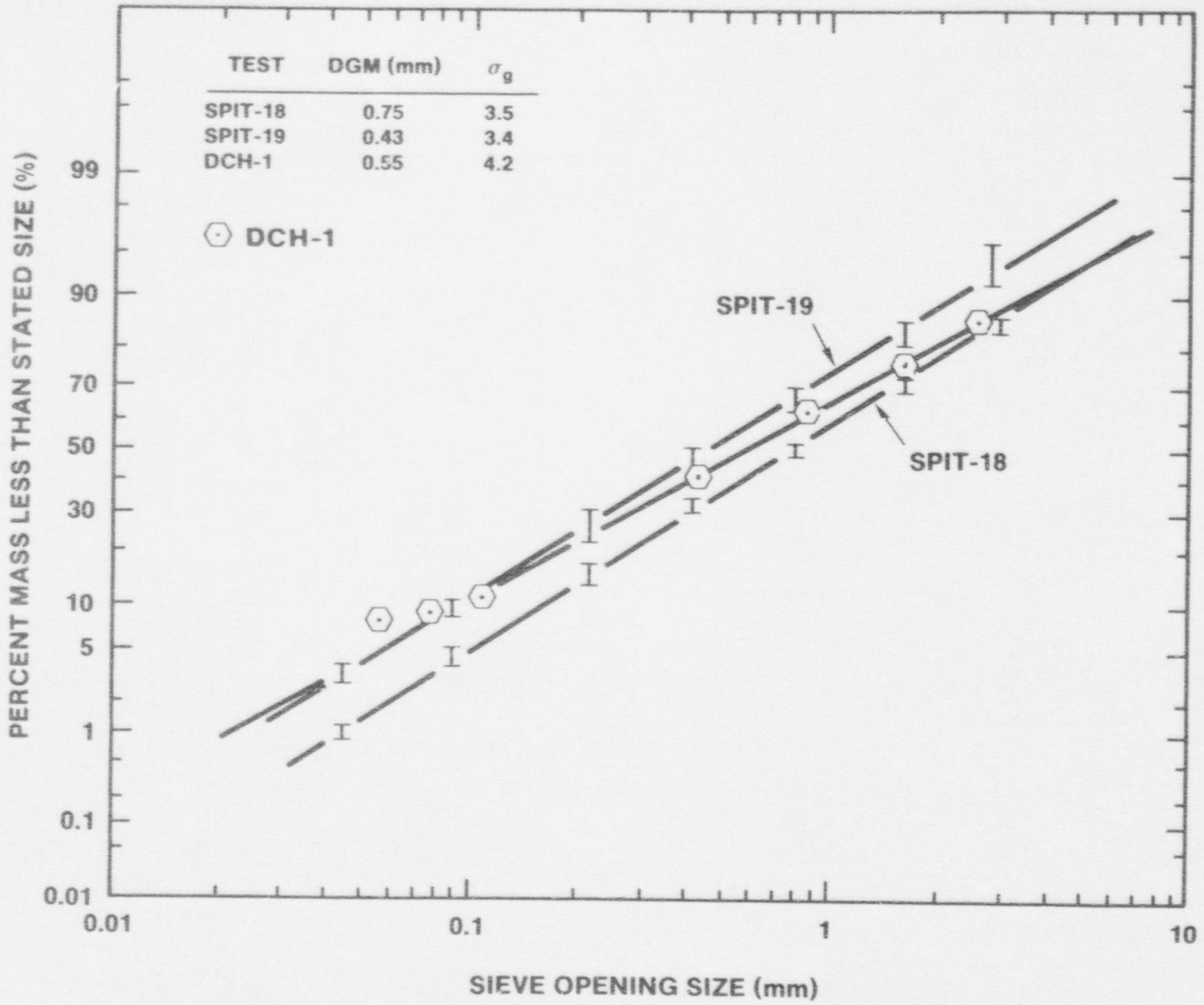

Figure 14. Particle Size Distribution from the DCH-1, SPIT-18, and SPIT-19 Tests

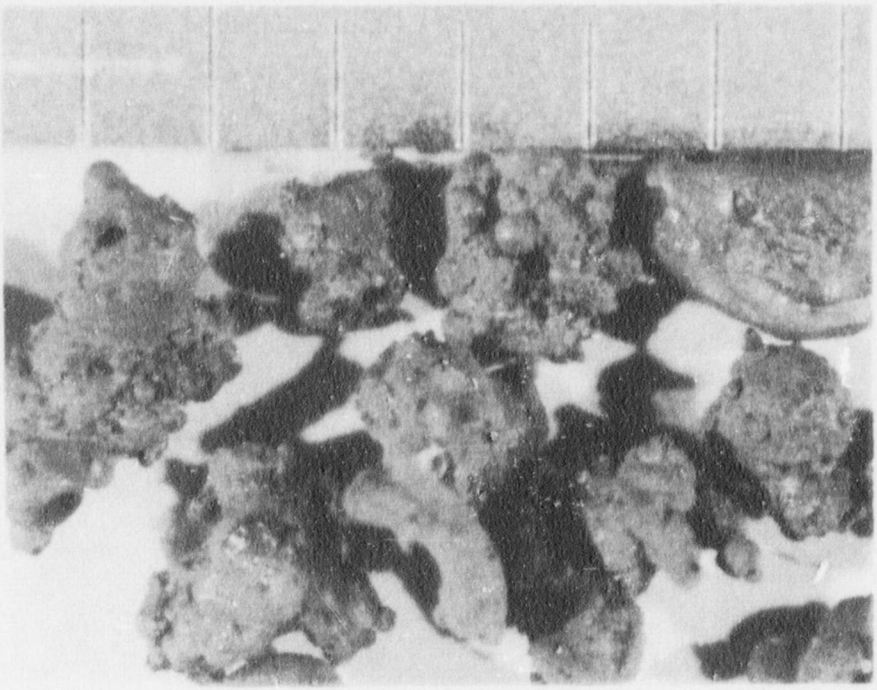

(a) > 2.38 mm

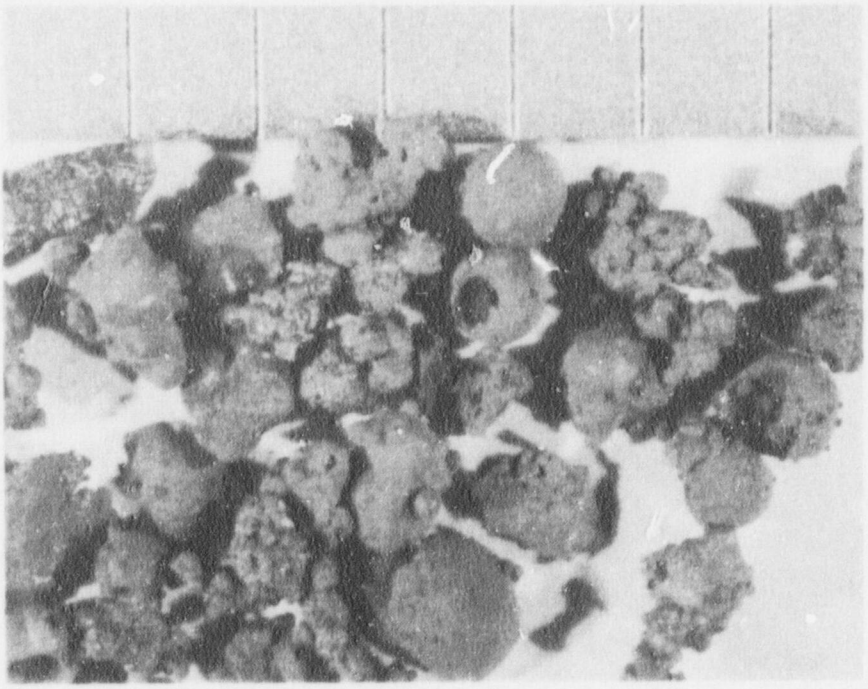

(b) 1.60 - 2.38 mm

Figure 15. Photographs of Collected Debris from the DCH-1 Experiment (1-mm Scale Marking)

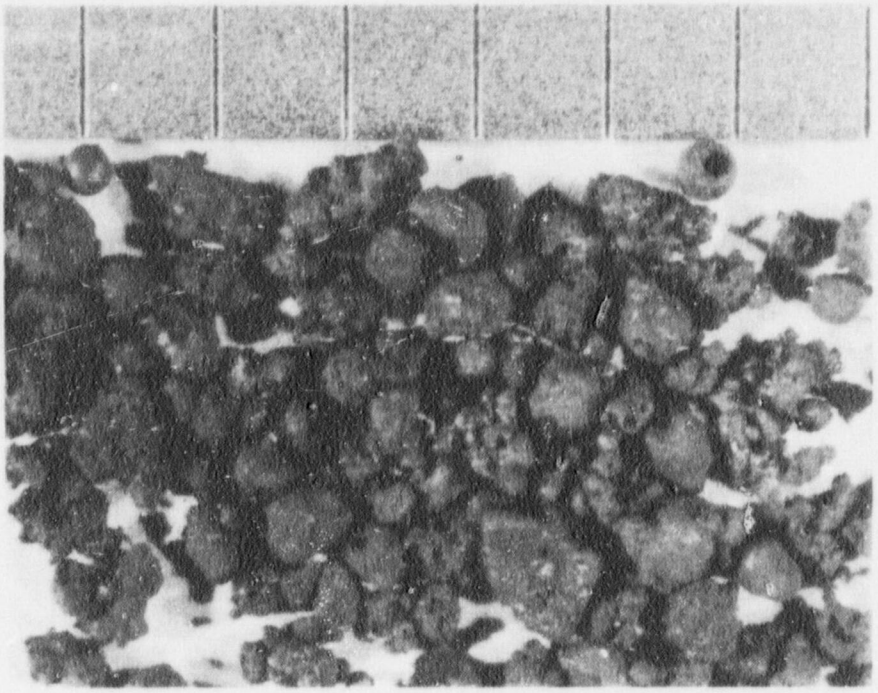

(c) 0.85 - 1.60 mm

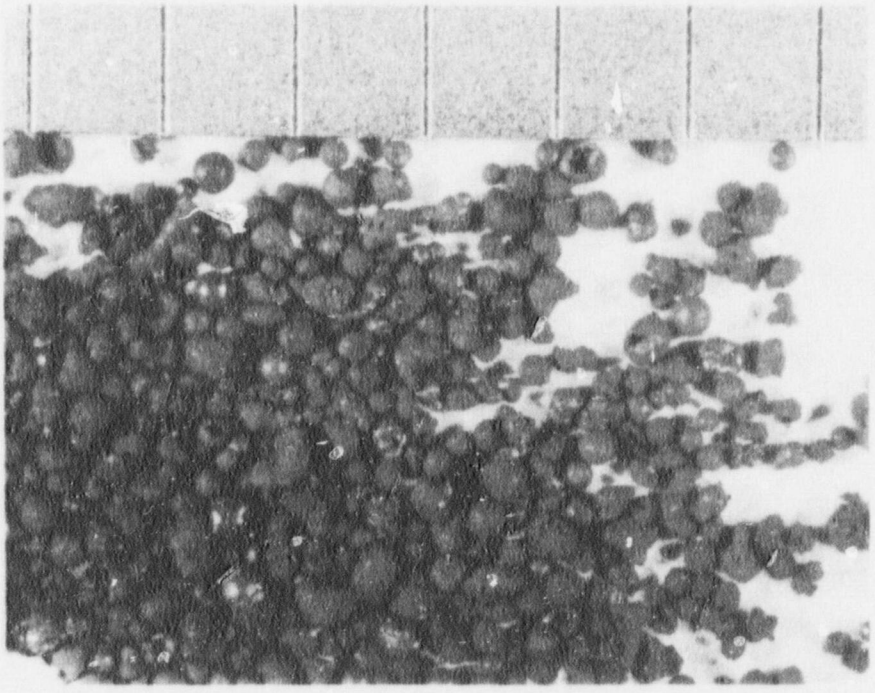

(d) 0.417 - 0.85 mm

Figure 15. (Continued)

TABLE 8
Qualitative Appearance of Collected Debris

Size (mm)	Description
>2.38	Mostly large agglomerates (>1 mm) with rough exterior appearance with some shrink holes, other very irregular shapes and some smooth spheres.
1.60-2.38	Irregular agglomerates (~1 mm) of smaller particles, some irregular shapes with smooth external surfaces, some spheres with shrink holes and some with small particles attached.
0.85-1.60	Similar to above except more spheres present, spheres differ in diameter throughout the size range.
0.417-0.85	Almost totally spheres and small irregular (angular) shapes, shrink holes obvious in many spheres.

E. Chamber Gas Composition

The composition of the chamber atmosphere was sampled before and after debris dispersal to determine the oxygen consumed by the oxidation of the metallic melt particles. Each sample bottle withdrew 50 ml from the chamber. Cycling time was determined by the valve actuation interval, or approximately 3-5 s per sample. Gas chromatography was then used to determine the chemical species of the sample. Figure 16 shows the oxygen concentration on a volume percent basis versus the time the sample was obtained. The results have not been corrected to account for the effect of the nitrogen gas ejected into the chamber from the melt generator or the difference in the chamber pressure for the samples taken shortly after debris dispersal. Both of these effects were estimated to be small contributors to the overall uncertainty of the method.

The results given in Figure 16 clearly show that oxygen consumption occurred. The first samples following debris dispersal indicate that the consumption did not occur immediately, but over a period of a few minutes. This behavior

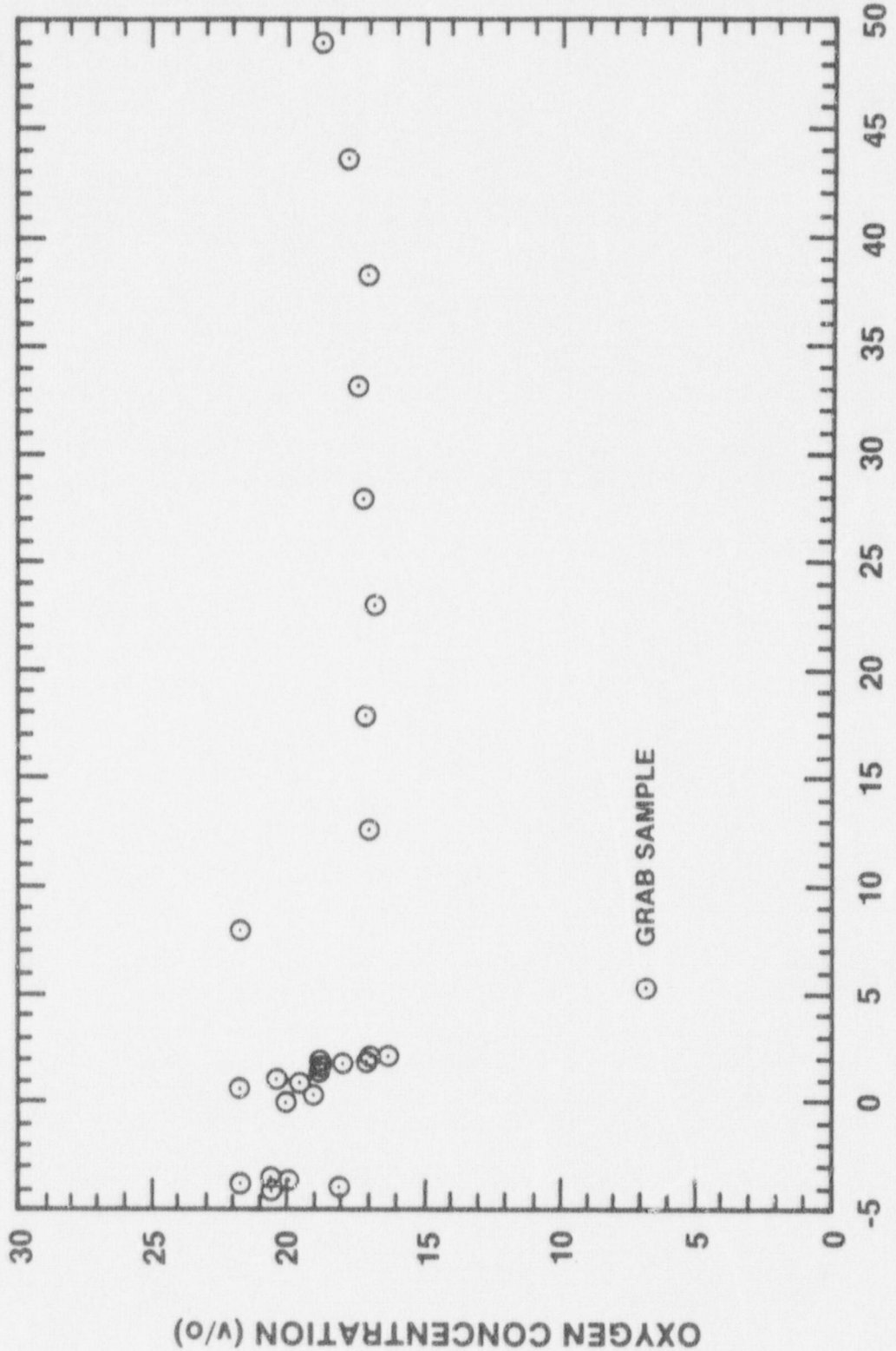

Figure 16. Oxygen Gas Concentration

was caused by the "dead volume" of gas within the sampling line. It was estimated that 5-8 samples were required before the gas was representative of that in the atmosphere after debris ejection. The initial value of approximately 20 v/o was disturbingly inconsistent considering that it was only atmospheric composition. The cause of the inconsistency was not obvious although residual oils and other contaminants in the lines may have contributed to the observed variation.

At approximately 12 min, the data became more consistent at about 16 v/o. The chamber remained at this level until after 40 min when the oxygen appeared to increase. The limited volume of the individual collection bottles made them particularly sensitive to the presence of contaminants in the sample. This may have been the cause of the scatter in the data prior to the test before the sample line was cleared.

F. Aerosol Measurements

Aerosol samples were taken in the Surtsey chamber during the first 40 min following the ejection of debris. The sampling time intervals, locations, and calculated concentrations are given in Table 9. The locations correspond to those defined in Table 1.

TABLE 9
Aerosol Measurements

Device	Location	Sample Time (s)	Collected Mass (mg) w/o PS*	Collected Mass (mg) Total	Avg Chamber Temp (K)	Avg Chamber Press (MPa)	Sampled Gas Volume (l)**	Calculated Concentration (g/m^3)
Impactor								
A	E-2	15-45	558	863	455	0.13	11.35	49-76
B	E-2	15-45	500	707	455	0.13	7.8	64-91
E	E-4	15-45	23.3	52.2	455	0.13	11.35	2.1-4.6
F	E-4	15-45	16.0	26.9	455	0.13	7.8	2.1-3.5
C	E-2	315-345	68.4	98.8	300	0.08	7.5	4.6-6.6

(Continued)

TABLE 9 (Continued)

Device	Location	Sample Time (s)	Collected Mass (mg) w/o PS*	Collected Mass (mg) Total	Avg Chamber Temp (K)	Avg Chamber Press (MPa)	Sampled Gas Volume (l)**	Calculated Concentration (g/m^3)
D	E-2	315-345	54.6	98.2	300	0.08	5.15	5.3-8.7
G	E-4	315-345	15.9	33.2	300	0.08	7.5	1.1-2.2
H	E-4	315-345	15.4	24.6	300	0.08	5.15	1.5-2.4
Cyclone								
1	E-4	15-2463	-	1327.2	300	0.08	620.0	2.1
Filter								
A	E-2	15-30	-	2.7	485	0.14	1.8	1.5
G	E-4	15-30	-	-	485	0.14	1.8	-
B	E-2	30-45	-	37.8	424	0.12	1.6	24.0
H	E-4	30-45	-	10.5	424	0.12	1.6	6.7
C	E-2	165-195	-	27.1	310	0.09	2.3	12.0
I	E-4	165-195	-	46.6	310	0.09	2.3	21.0
D	E-2	315-345	-	-	300	0.08	2.2	-
J	E-4	315-345	-	16.1	300	0.08	2.2	7.3
E	E-2	1344-1404	-	8.6	300	0.08	4.4	2.0
K	E-4	1344-1404	-	15.1	300	0.08	4.4	3.4
F	E-2	15-2463	-	390.4	300	0.08	181.9	2.1
L	E-4	2403-2463	-	11.7	300	0.08	4.4	2.7

* PS - preseparator
** Actual volume of gas sampled at the chamber condition

The measured aerosol concentration varied widely over time and between sampling location. This indicated a considerable inhomogeneity in aerosol concentration in the chamber. The number of samples was increased (and the sampling statistics improved) by grouping together the samples taken for the first 195 s of the test. This procedure was justified by a simple analysis of stirred settling in the Surtsey chamber.

$$F = \exp[-kA\Delta t/V]$$

where:

F = fraction of initial concentration (0.90)

k = particle deposition velocity

A = horizontal area of chamber (12.5 m^2)

Δt = elapsed time (195 s)

V = chamber volume (103 m^3)

thus:

$$k = 4.45 \text{ m/s} .$$

The calculated value of k is the settling velocity corresponding to a 12-μm aerodynamic diameter particle. This calculation indicates that at the end of 195 s, 90% of the 12-μm diameter and smaller particles were still airborne.

Table 10 contains the measured sample concentrations, their means and standard deviations, and the 95% confidence intervals obtained from the standard deviation and Student-t statistics. The impactor samples were used neglecting the larger material collected in the preseparators (values of concentration including the preseparator material are indicated in parentheses). The sampler is identified with a letter designation and the sampling interval is given relative to the time of ejection. The cascade impactors samples A and B were anomalously high and have not been included in these results. Examination of the concentration measurements at 1343 and 2403 s and the 15 to 2463-s interval suggests that the initial concentration may have been greater than 2 g/m^3. If this is used as a lower bound, the initial aerosol concentration in the chamber can be reasonably assumed to lie between 2 and 18.6 g/m^3.

TABLE 10
Calculated Aerosol Concentration

Sampler and Time (s)	Concentration* (g/m^3)	Mean Value (g/m^3)	Standard Deviation (%)	Range of 95% Interval (g/m^3)
FA 15-30	1.52			
FB 30-45	24.0			
FH 15-45	6.7			
FC 165-195	12.0			
FI 315-345	21.0			
IE 1343-1404	2.1 (4.6)			
IF 2403-2463	2.1 (3.5)			
		9.9 (10.5)**	9.4 (8.9)	1.2 to 18.6 (2.3 to 18.7)
FJ 315-345	7.3			
IC 315-345	4.6 (6.6)			
ID 315-345	5.3 (8.7)			
IG 315-345	1.1 (2.2)			
IH 315-345	1.5 (2.4)			
		4.0 (5.4)	2.6 (3.0)	0.8 to 7.2 (1.7 to 9.1)
FE 1343-1404	2.0			
FK 1343-1404	3.4			
		2.7	1.0	
FL 2403-2463	2.7			
FF 15-2463	2.1			
C1 15-2463	2.1			

* F=Filter, I=impactor, C=cyclone
** Values in parentheses include mass in pre-separator

The calculated concentrations were the values obtained from the measured mass of aerosol and the volume of gas that passed

through the sampling device. The total suspended mass was obtained from the product of the chamber volume and the concentration. Because the chamber volume was nominally 103 m^3, the calculated aerosolized mass was in the range of 0.2 to 1.9 kg. These values represent 1.7 to 16% of the mass of debris recovered from outside the cavity.

Figure 17 shows the suspended aerosol mass in the chamber as a function of time. The data points at 23 and 40 min are plotted individually because there were too few to yield statistically significant averages or confidence intervals.

The cascade cyclone and filter F gave a 40-min sample average. The close agreement between the results from these devices suggested reasonable accuracy. These data indicated an initially high aerosol concentration (~10 g/m^3), which fell off very rapidly at first and then slowed. This was consistent with the bimodal source term where the large mode concentration dominates the early time behavior. The large particles rapidly fall out of suspension and take some of the smaller particles by interception and settling.[3] The remaining small-mode concentration then decayed more slowly.

The aerosol mass distribution was measured at two times in the chamber (15-45 and 315-345 s). A simultaneous sample was taken at both the upper and lower locations. Each sample consisted of two impactors, one with a flow rate of 15 l/min and the other at 10 l/min. This gave staggered cutpoints and the algebraic combination of the results from the two impactors yielded a distribution with greater resolution than either impactor separately. The results from impactors E and F (15-45 s at lower location), C and D (315-345 s, lower), and G and H (315-345 s, upper) are plotted in Figures 18, 19, and 20, respectively. In these figures D_p is the equivalent aerodynamic diameter, DGM is the geometric mass mean diameter, and σ_g is the geometric standard deviation. Impactors A and B were overloaded with material so that the individual stage weights could not be determined.

The 15-45 s distribution data measured by impactors E and F (Figure 18) was distinctly bimodal with peaks at 1 and >10-μm aerodynamic equivalent diameter. A third mode at 5 μm may also be present. Approximately one-half of the total mass was less than 10-μm diameter. The smaller mode consisted primarily of floculated material and was described well by a lognormal distribution with a geometric mass median aerodynamic diameter of 1 μm and a geometric standard deviation between 1.7 and 1.9.

The distributions obtained from samples taken five minutes later (C & D - Figure 19, G & H - Figure 20) indicated a mode at less than 10 μm. These data were affected by overloading of the

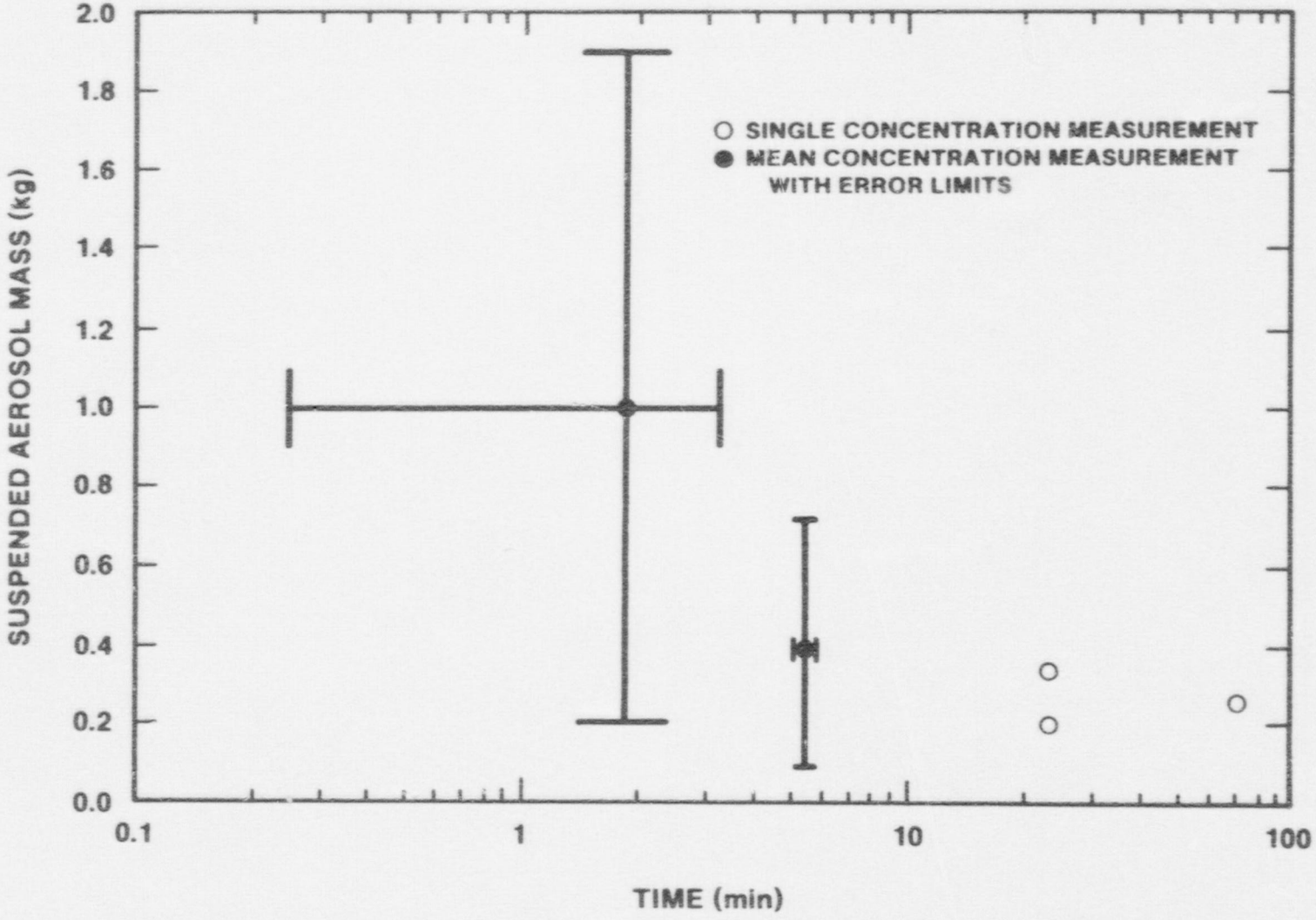

Figure 17. Suspended Aerosol Mass

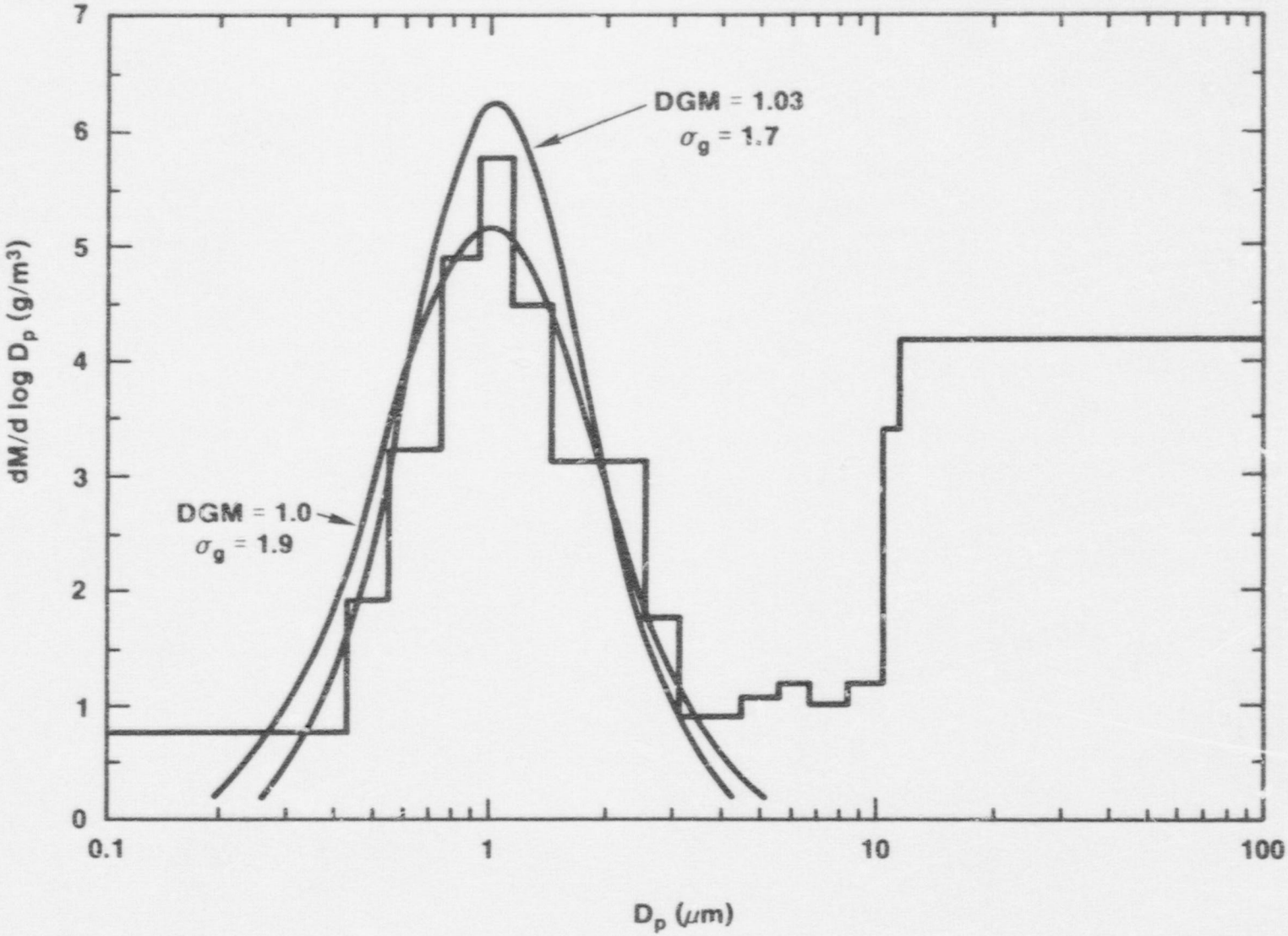

Figure 18. Aerosol Mass Distribution - Impactors E and F

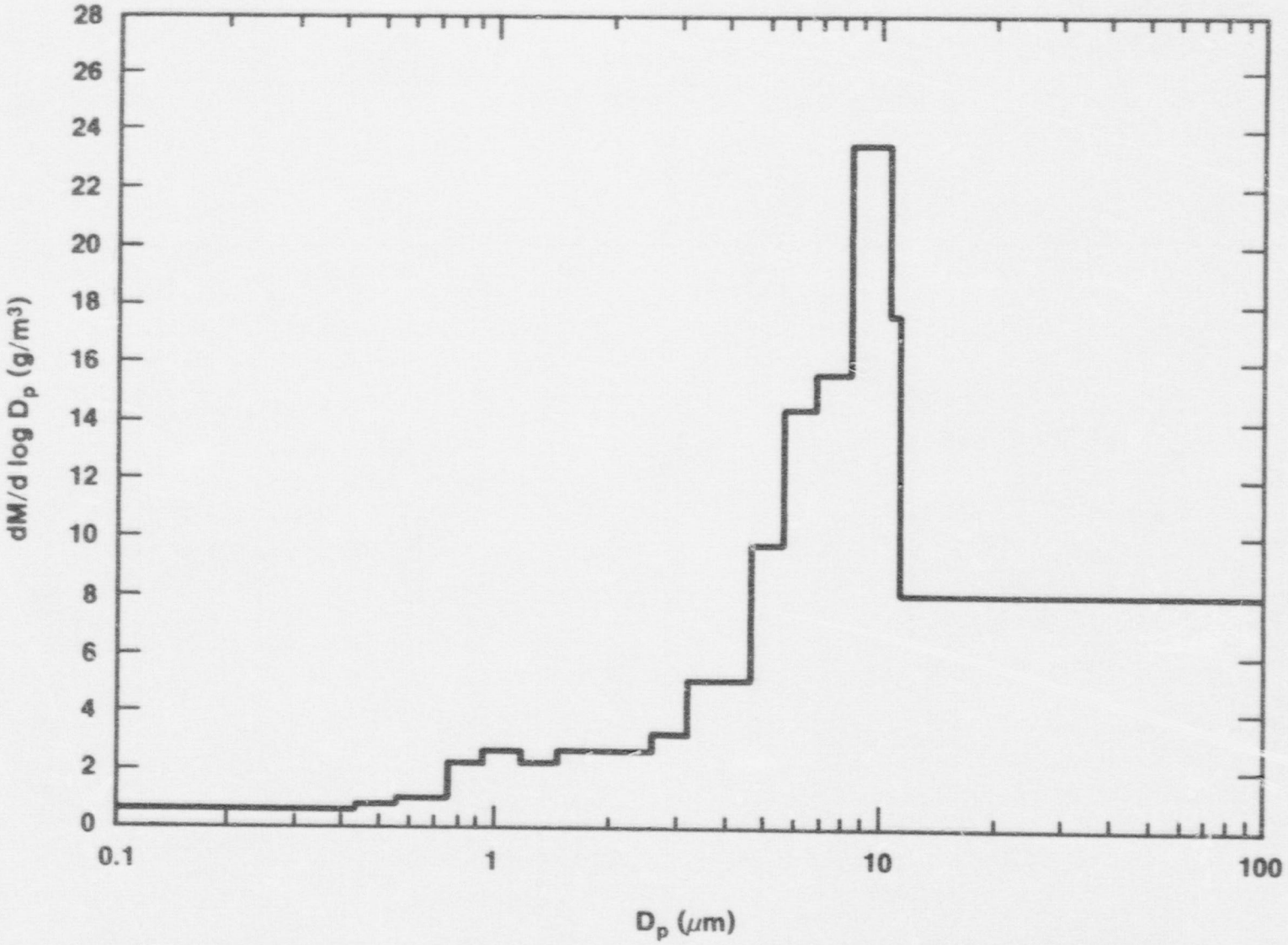

Figure 19. Aerosol Mass Distribution - Impactors C and D

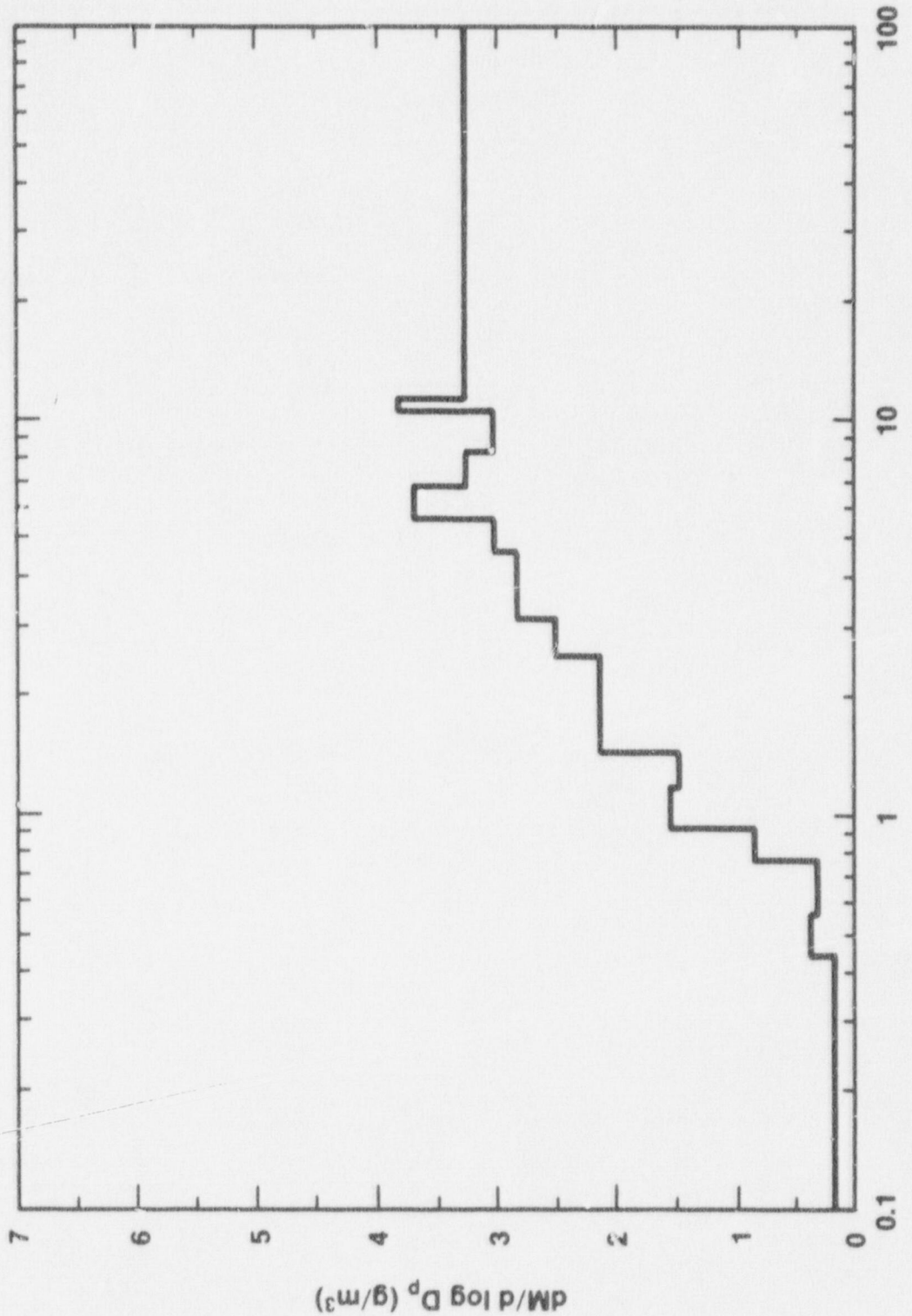

Figure 20. Aerosol Mass Distribution - Impactors G and H

sampler. The overloading was attributed to the physical bulk of the collected material. The aerosol had a high void fraction that resulted in large collection volumes at each stage that appeared to interfere with the normal flow patterns through the devices.

Data were not obtained from the transmissometer (photometer) because the internal light source failed shortly after melt ejection.

A steel box of approximately one cubic meter volume was used to dilute the aerosol samples drawn from the chamber for the APS. A cascade impactor was also used to provide a mass distribution along with the number distribution of the APS. The simultaneous measurement of these distributions and the material density yield the aerodynamic shape factor. The dynamic shape factor relates aerodynamic equivalent diameter and the mass equivalent diameter. For a particle of given mass, a larger shape factor means that it will fall slower. Large shape factors mean a larger or heavier particle to be suspended longer.

Preliminary examination of the data from 4 hr after melt ejection indicated a bimodal mass distribution with modes at about 1 and 6-μm aerodynamic diameter. Figures 21 and 22 are the mass and number distributions, respectively, from the impactor and APS. The dynamic shape factor (χ) has not yet been determined pending further development of the analysis technique.

Deposition of aerosol on the walls of the chamber was estimated by vacuuming six separated areas and collecting the material on a filter. Table 11 gives the results of this process. The mean surface concentration was 0.183 $\pm$0.029 mg/cm^2. Based on the total vertical surface area, it was estimated that 128 to 180 g of aerosol was deposited on the walls of the vessel.

TABLE 11
Aerosol Wall Deposition

Filter Location*	Collected Mass (mg)	Wall Area (cm^2)	Surface Concentration (mg/cm^2)
70/2	41.03	231	0.178
140/2	33.41	169	0.198

(Continued)

TABLE 11 (Continued)

Filter Location*	Collected Mass (mg)	Wall Area (cm^2)	Surface Concentration (mg/cm^2)
190/5	40.34	216	0.187
280/5	30.08	132	0.228
0/4	22.35	150	0.149
130/4	20.49	132	0.155
		Mean	0.183

* Location is given by compass degrees from due North (first number) and level (second number) as given on Figure 1.

The filter samples H, I, and F were analyzed by ICP (Inductively Coupled Plasma) emission spectroscopy to give elemental composition of the collected aerosol. The results are given in Table 12.

The ICP results show excellent similarity between the three samples. This similarity suggests that the aerosol was formed from the same processes and materials. While concentration in the chamber appeared to be heterogeneous, the composition was quite homogeneous. The ratio of Fe to Al in the aerosol was several times higher than that of the bulk melt. This suggests that most of the collected aerosol mass came from vapor condensation and little from melt fragmentation. The mass distribution measured at 15 to 45 s (Figure 18) showed a distinctly bimodal character with the smaller vapor condensation mode at about 1 μm. The larger melt fragmentation aerosol was greater than 10 μm mean diameter, a size not efficiently collected by the filters.

Release fractions were estimated from the filter samples by assuming that the devices contained mostly sub-10 μm aerosol particles and that the collected material reflects the composition of the entire chamber. Given these assumptions and the total mass of the vapor condensation aerosol, the release fractions of the melt constituents were calculated using the known composition of the brass fusible plug.

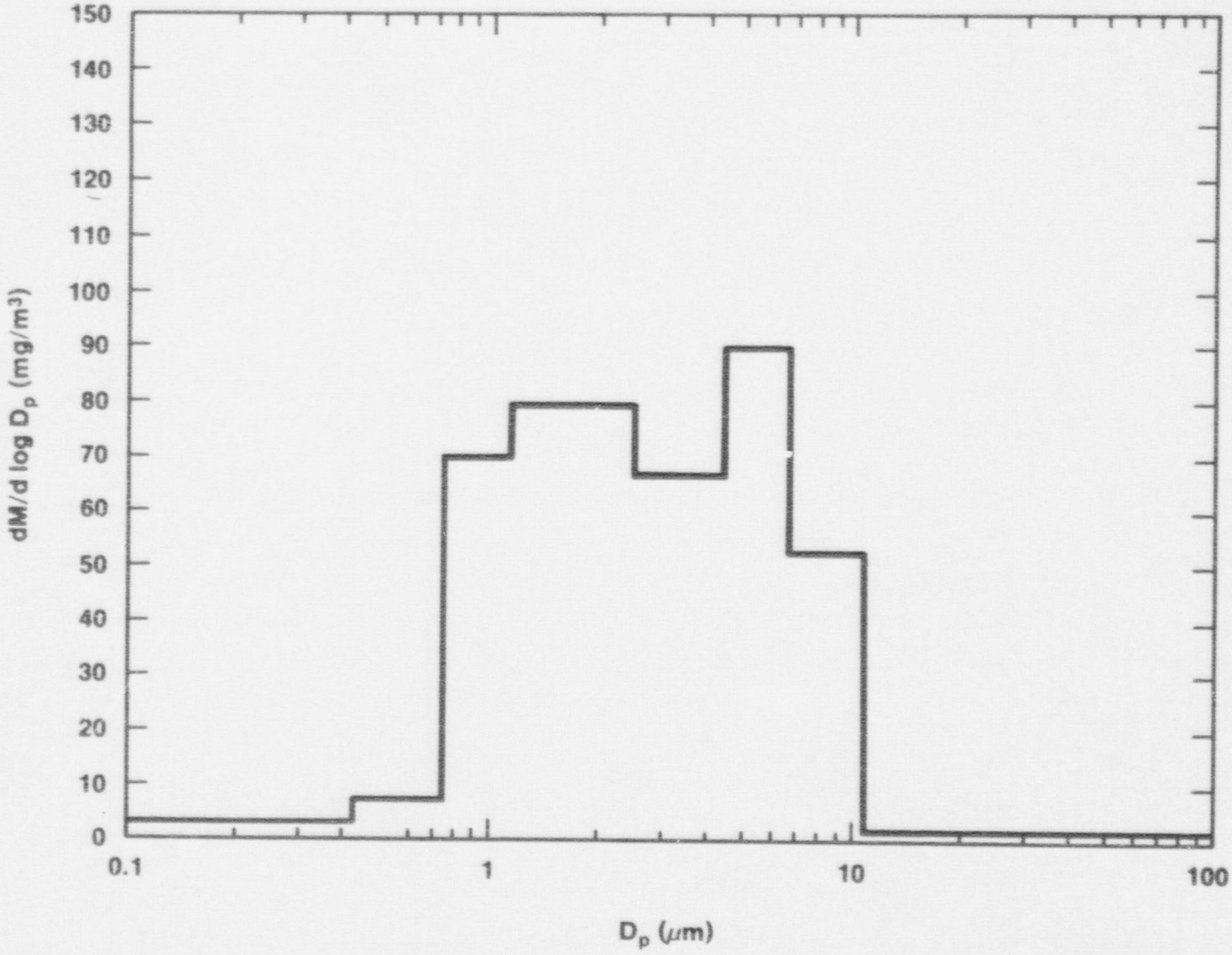

Figure 21. Aerosol Mass Distribution - APS and Impactors

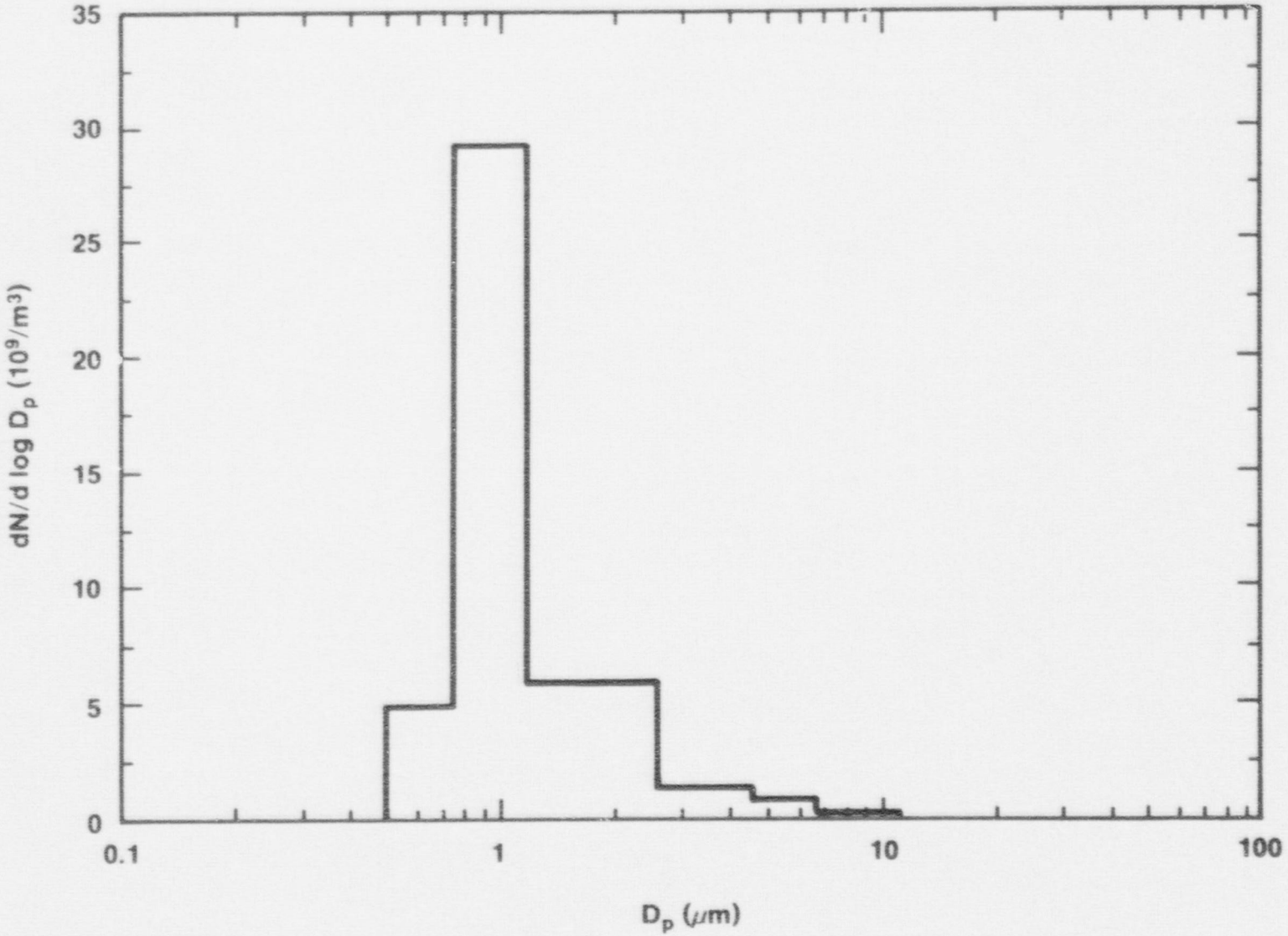

Figure 22. Aerosol Number Distribution - APS and Impactors

TABLE 12
Aerosol Composition Analysis

Element	Sample H*	Sample I**	Sample F+
	(Elemental Weight Percent)		
Fe	38.8	36.7	36.1
Al	7.45	3.5	3.1
Zn	8.7	12.2	12.6
Cu	4.3	5.9	6.1
Pb	0.70	1.0	1.0
Si	3.0	2.8	4.15
K	0.32	0.75	0.80
Ca	0.34	0.10	0.08
Mo	0.85	1.1	1.15
Ni	0.50	0.50	0.51
Nb	0.18	0.07	0.06
Ba	0.14	0.11	0.10
La	0.04	0.03	0.03

* Sampler H @ 30-45 s
** Sampler I @ 165-195 s
+ Sampler F @ 15-2463 s

The brass used to make the fusible plug consisted of 62 w/o Cu, 35 w/o Zn, and 3 w/o Pb. The ratio of Zn to Pb was the same in the aerosol as in the raw material while the ratio of Zn to Cu was not. Both Zn and Pb have boiling points below the temperature of the thermite reaction products while the Cu boiling temperature is higher. If it is assumed that all of the Zn and Pb were vaporized and available for aerosol formation, then the assumption of compositional homogeneity would allow determining the total vaporization aerosol.

Considering that the brass plug contained 0.103 g of Zn, then the 8.7 w/o of Zn in sampler H indicates 1.18 kg of vapor condensation aerosol, sampler I - 0.84 kg, and sampler F - 0.82 kg. The average of these three calculations is 0.95 kg, which is in remarkable agreement with the 0.99-kg mean initial aerosol

concentration (Figure 17). The 95% confidence interval for these three compositions is 0.55 kg to 1.45 kg of suspended vapor condensation aerosol or 0.95 kg ±53%.

Release fractions were calculated for the relocated debris as the mass released by vaporization divided by the mass in the initial melt for the element of interest. The relocated melt debris was calculated to be between 46% to 56% of the original mass of 21.115 kg. Table 13 presents the calculated release fractions for the principal elements of the aerosol.

TABLE 13
Elemental Aerosol Release Fractions

Element	Mass In Relocated Debris[1] (g)	Mass In Aerosol[2] (g)	Release Fraction[3] (%)
Fe	5610	353	6.3
Al	2430	44	1.81
Mo	51.5	9.8	19.0
Ni	51.0	4.8	9.4
Nb	51.0	0.98	1.92
Ba	73.7	1.11	1.51
La	51.3	0.35	0.68

[1]Uncertainty in relocated mass = ±10%
[2]Uncertainty in aerosol mass = ±53%
[3]Resulting uncertainty in release fraction = ±54%

The large uncertainty in the calculated release fractions (±54%) arises primarily from the uncertainty in the aerosolized mass that was caused by the limited number of filters analyzed. Additional but unquantified uncertainty may be from vaporization release from ejected debris that was retained in the cavity and from mechanically produced melt fragmentation particles collected on the filters.

VI. CONCLUSIONS

The results from the DCH-1 experiment provided well characterized data to support the development of models needed to quantify high pressure melt ejection, radionuclide release, and direct heating of the containment atmosphere. Data included chamber pressure rise, debris and aerosol characteristics and release of radionuclide mocks from the relocated melt debris.

Recorded pressure in the chamber was on the order of 0.1 MPa (15 psig), from 11.6 kg of dispersed debris. The debris was in the form of small particles with a broad lognormal distribution and a mass mean size of 0.55 mm. The debris size matched the material collected from previous 1:20 scale cavity experiments. Aerosol measurements indicated that a substantial portion of the discharged mass (1.7% to 16%) was less than 10-μm diameter. Release fractions from relocated melt debris were determined from the measured data. The calculated aerosol concentration varied significantly in time and with sampler location, although the composition of the aerosol appears to have been homogeneous.

VII. REFERENCES

1. W. W. Tarbell, et al., Pressurized Melt Ejection Into Scaled Reactor Cavities, Sandia National Laboratories, Albuquerque, NM, NUREG/CR-4512, SAND86-0153, Oct 1986.

2. M. Pilch and W. W. Tarbell, Preliminary Calculations on Direct Heating of a Containment Atmosphere by Airborne Core Debris, Sandia National Laboratories, Albuquerque, NM, NUREG/CR-4456, SAND85-2439, Jul 1986.

3. N. A. Fuchs, The Mechanics of Aerosols, Pergamon Press, 1964.

Distribution:

U.S. Government Printing Office
Receiving Branch (Attn: NRC Stock)
8610 Cherry Lane
Laurel, MD 20707
510 copies for R3, R4, R7

U.S. Nuclear Regulatory Commission (22)
Office of Nuclear Regulatory Research
Washington, DC 20555
Attn: E. S. Beckjord
C. N. Kelber
M. Silberberg
G. Marino
L. Chan
C. Ryder
R. W. Wright
T. Walker
R. O. Meyer
J. Mitchell
S. B. Burson
T. Lee (5)
M. Cunningham
J. Murphy
P. Wood
T. Speis
W. Lyon
F. Eltawilla

U.S. Nuclear Regulatory Commission (6)
Office of Nuclear Regulatory Regulation
Washington, DC 20555
Attn: L. G. Hulman
P. Easky
J. Rosenthal
B. Hardin
Z. Rosztoczy
R. Barrett

U.S. Department of Energy (2)
Albuquerque Operations Office
P.O. Box 5400
Albuquerque, NM 87185
Attn: J. R. Roeder, Director
J. A. Morley, Director
For: C. B. Quinn
R. N. Holton

U.S. Department of Energy
Office of Nuclear Safety Coordination
Washington, DC 20545
Attn: R. W. Barber

Electric Power Research Institute (4)
3412 Hillview Avenue
Palo Alto, CA 94303
Attn: R. Vogel
R. Ritzman
W. Lowonstein
R. Sehgal

Brookhaven National Laboratory (5)
Upton, NY 11973
Attn: R. A. Bari
T. Pratt
N. Tutu
G. Greene
T. Ginsberg

Professor R. Seale
Department of Nuclear Engineering
University of Arizona
Tucson, AZ 85721

Oak Ridge National Laboratory
P.O. Box Y
Oak Ridge, TN 37830
Attn: T. Kress

K. Holtzclaw
General Electric - San Jose
Mail Code 682
175 Kurtner Avenue
San Jose, CA 95125

Argonne National Laboratory (5)
9700 South Cass Avenue
Argonne, IL 60439
Attn: J. Rest
C. Johnson
L. Baker, Jr.
D. Cho
B. Spencer

Cathy Anderson
Nuclear Safety Oversight Commission
1133 15th St., NW
Room 307
Washington, DC 20005

Battelle Columbus Laboratory (3)
505 King Avenue
Columbus, OH 43201
Attn: P. Cybulskis
R. Denning
J. Gieseke

J. E. Antill
Berkeley Nuclear Laboratory
Berkeley GL 139 PB
Gloucestershire
ENGLAND, U.K.

W. G. Cunliffe
Bldg. 396
British Nuclear Fuels, Ltd.
Springfields Works
Salwick, Preston
Lancashire
ENGLAND, U.K.

R. Deem
Power Authority State of NY
10 Columbus Circle
New York, NY 10019

Professor Agustin Alonso
E.T.S. Ingenieros Industriales
Jose Gutierrez Abascal, 2
28006 Madrid, SPAIN

Dr. Alfonso Perez
Department de Seguridad Nuclear
Junta de Energia Nuclear
Avenida Complutense, 22
Madrid - 3, SPAIN

R. Sherry
JAYCOR
P.O. Box 85154
San Diego, CA 92138

Ktech Corp. (4)
901 Pennsylvania NE
Albuquerque, NM 87110
Attn: R. E. Blose
M. S. Oliver
J. Jackson
J. W. Ross

Los Alamos National Laboratories
P.O. Box 1663
Los Alamos, NM 87545
Attn: M. Stevenson

UCLA (2)
Nnuclear Energy Laboratory
405 Hilgaard Avenue
Los Angeles, CA 90024
Attn: I. Catton
D. Okrent

University of Wisconsin
Nuclear Engineering Department
1500 Johnson Drive
Madison, WI 53706
Attn: M. L. Corradini

EG&G Idaho
Willow Creek Building, W-3
P.C. Box 1625
Idaho Falls, ID 83415
Attn: R. Hobbins

Battelle Pacific Northwest Laboratory
P.O. Box 999
Richland, WA 99352
Attn: M. Freshley

Wiktor Frid
Swedish State Power Board
S-162 FACH 87 VALLINGBY
SWEDEN

W. Stratton
2 Acoma Lane
Los Alamos, NM 87544

Gesellschaft fur Reaktorsicherheit (GRS)
Postfach 101650
Glockengrasse 2
5000 Koeln 1
Federal Republic of GERMANY

Kraftwerk Union
Hammerbacher Strasse 1214
Postfach 3220
D-8520 Erlangen 2
Federal Republic of GERMANY
Attn: Dr. M. Peehs

UKAEA
Reactor Development Division (5)
Winfrith, Dorchester
Dorset DT2 8DH
ENGLAND, U.K.
Attn: R. Potter
A. Nichols
B. Bowsher
P. Smith
T. Butland

Nucleare e della Protezione Sanitaria (DISP) (2)
Ente Nazionnle Energie Alternative (ENEA)
Viale Regina Margherita, 125
Casella Postale M. 2358
I-00100 Roma A.D., ITALY
Attn: Mr. Manilia
Mr. G. Petrangeli

Dr. K. J. Brinkman
Reactor Centrum Nederland
1755 ZG Petten
THE NETHERLANDS

Dr. S. J. Niemczyk
1545 18th Street, NW
#112
Washington, DC 20036

Kernforschungszentrum Karlsruhe
Postfach 3640
75 Karlsruhe
Federal Republic of GERMANY
Attn: H. Rininsland

Mr. H. Bairiot, Chief
Department LWR Fuel
Belgonucleaire
Rue de Champde Mars. 25
B-1050 Brussels, BELGIUM

Japan Atomic Energy Research Institute
Tokai-Mura, Naka-Gun
Ibaraki-Ken 319-11
JAPAN
Attn: S. Saito

Wang Lu
TVA
400 Commerce, W9C157-CK
Knoxville, TN 37902

M. Fontana
Director, IDCOR Program
ENERGEX
575 Oak Ridge Turnpike
Oak Ridge, TN 37830

Fauske and Associates, Inc. (2)
16W070 West 83rd Street
Burr Ridge, IL 60521
Attn: R. Henry
M. Plys

Peter Bieniarz
Risk Management Associates
2309 Dietz Farm Road, NW
Albuquerque, NM 87107

Dr. K. Soda
Manager,
Chemical Engineering Safety Laboratory
Department of Nuclear Fuel Safety
Japan Atomic Energy Research Institute
Tokai-Muri, Naku-Gun, Ibaraki-Ken
319-11
JAPAN

K. Sato, Director
Department of Reactor Safety Research
Japan Atomic Energy Research Institute
Tokai-Mura, Naka-Gun, Ibaraki-Ken
JAPAN

P. Fehrenbach
Atomic Energy Canada, Ltd.
Chalk River, Ontario
CANADA KOJ IJO

M. Hayns
UKAEA
Safety and Reliability Directorate
Wigshaw Lane
Culcheth
Warrington WA3 4NE
Cheshire,
ENGLAND, U.K.

J. R. Mathews
Aere Harwell
Didcot
Oxfordshire OX11 ORA
ENGLAND, U.K.

F. Briscoe
UKAEA Culham Laboratory
Abingdon
Oxfordshire OX14 3DB
ENGLAND, U.K.

H. J. Teague (3)
UKAEA
Safety and Reliability Directorate
Wigshaw Lane
Culcheth
Warrington, WA3 4NE
ENGLAND, U.K.

M. Jankowski
IAEA
Division of Nuclear Reactor Safety
Wagranerstrasse 5
P.O. Box 100
A/1400 Vienna, AUSTRIA

Statens Karnkraftinspektion
L. Hammer
P. O. 27106
S-10252 Stockholm, SWEDEN

Studsvik Energiteknik AB
K. Johansson
S-611 82 Nykoping, SWEDEN

Atomic Energy Canada Ltd.
M. Notley
Chalk River, Ontario
CANADA KOJ 1JO

Atomic Energy Canada Ltd. (2)
Pinawa, Manitoba
CANADA ROE 1LO
Attn: H. Rosinger
D. Wren

Korea Adv Energy Research Inst
H. R. Jun
P.O. Box 7
Daeduk-Danji
Choong-Nam, KOREA

Institute of Nuclear Energy Research
Sen-I Chang
P.O. Box 3
Lungtan
Taiwan 325, Republic of CHINA

3141	S. A. Landenberger (5)
3151	W. L. Garner
6400	D. J. McCloskey
6411	A. S. Benjamin
6412	A. L. Camp
6415	F. E. Haskin
6420	J. V. Walker
6421	P. S. Pickard
6422	D. A. Powers (5)
6422	F. E. Arellano
6422	J. E. Brockmann (2)
6422	E. R. Copus
6422	R. Gomez
6422	T. M. Kerley
6422	D. A. Lucero
6422	W. W. Tarbell (5)
6425	W. J. Camp
6425	M. Pilch (2)
6425	N. Yamano
6427	M. Berman
6427	L. Pong
6427	B. Marshall
6440	D. A. Dahlgren
6442	W. A. Von Riesemann
6419	K. D. Bergeron
6419	D. E. Carroll
6419	J. Tills
6419	K. E. Washington
6419	D. C. Williams
6454	G. L. Cano
6512	D. M. Ericson, Jr.
7530	T. B. Lane
7537	N. R. Keltner
8024	P. W. Dean

NRC FORM 335 (2-84) NRCM 1102, 3201, 3202

SEE INSTRUCTIONS ON THE REVERSE

U.S. NUCLEAR REGULATORY COMMISSION

BIBLIOGRAPHIC DATA SHEET

1 REPORT NUMBER (Assigned by TIDC, add Vol. No., if any)

NUREG/CR-4871

2 TITLE AND SUBTITLE

RESULTS FROM THE DCH-1 EXPERIMENT

3 LEAVE BLANK

4 DATE REPORT COMPLETED

MONTH	YEAR
May	1987

5 AUTHOR(S)

William W. Tarbell
John E. Brockmann
Marty Pilch
James W. Ross
Michael S. Oliver
Daniel A. Lucero
Frank E. Arellano
Richard D. Gomez
Thomas E. Kerley

6 DATE REPORT ISSUED

MONTH	YEAR
June	1987

7 PERFORMING ORGANIZATION NAME AND MAILING ADDRESS (Include Zip Code)

Sandia National Laboratories
Division 6422
Albuquerque, NM 87185-5800

8 PROJECT/TASK/WORK UNIT NUMBER

9 FIN OR GRANT NUMBER

FIN A1406

10 SPONSORING ORGANIZATION NAME AND MAILING ADDRESS (Include Zip Code)

USNRC
Office of Nuclear Regulatory Research
Division of Reactor System Safety

11a TYPE OF REPORT

SAND

b PERIOD COVERED (Inclusive dates)

12 SUPPLEMENTARY NOTES

13 ABSTRACT (200 words or less)

The DCH-1 (Direct Containment Heating) test was the first experiment performed in the Surtsey Direct Heating Test Facility. The test involved 20 kg of molten core debris simulant ejected into a 1:10 scale model of the Zion reactor cavity. The melt was produced by a metallothermic reaction of iron oxide and aluminum powders to yield molten iron and alumina. The cavity model was placed so that the emerging debris propagated directly upwards along the vertical centerline of the chamber.

Results from the experiment showed that the molten material was ejected from the cavity as a cloud of particles and aerosol. The dispersed debris caused a rapid pressurization of the 103-m^3 chamber atmosphere. Peak pressure from the six transducers ranged from 0.09 to 0.13 MPa (13.4 to 19.4 psig) above the initial value in the chamber. Posttest debris collection yielded 11.6 kg of material outside the cavity, of which approximately 1.6 kg was attributed to the uptake of oxygen by the iron particles. Mechanical sieving of the recovered debris showed a lognormal size distribution with a mass mean size of 0.55 mm. Aerosol measurements indicated a substantial portion (2 to 16%) of the ejected mass was in the size range less than 10 m aerodynamic equivalent diameter.

14 DOCUMENT ANALYSIS — a KEYWORDS/DESCRIPTORS

High Pressure Melt Ejection
Direct Containment Heating
DCH
HPME
Aerosol
Debris
Reactor Cavity
HIPS

b IDENTIFIERS/OPEN-ENDED TERMS

15 AVAILABILITY STATEMENT

16 SECURITY CLASSIFICATION

(This page)

(This report)

17 NUMBER OF PAGES

18 PRICE

☆ U.S. GOVERNMENT PRINTING OFFICE: 1987—773-049/41051